Stramski, D.; Reynolds, R.A.; Gernez, P.; Roettgers, R.; Wurl, O.:
Inherent optical properties and particle characteristics of the sea-surface microlayer.
In: Progress in Oceanography. Vol. 176 (2019) 102117.
First published online by Elsevier: 25.05.2019

https://dx.doi.org/10.1016/j.pocean.2019.05.009

Inherent optical properties and particle characteristics of the sea-surface microlayer

Dariusz Stramski[1*], Rick A. Reynolds[1], Pierre Gernez[2], Rüdiger Röttgers[3], and Oliver Wurl[4]

[1]*Marine Physical Laboratory, Scripps Institution of Oceanography, University of California San Diego, La Jolla, California 92093-0238, USA.*

[2]*Mer Molécules Santé, Université de Nantes, 2 rue de la Houssinière, 44322 Nantes, France.*

[3]*Institute of Coastal Research, Helmholtz-Zentrum Geesthacht, Centre for Materials and Coastal Research, Max-Planck-Str. 1, D-21502 Geesthacht, Germany.*

[4]*Carl-von-Ossietzky Universität Oldenburg, Institut für Chemie und Biologie des Meeres, Schleusenstrasse 1, 26382 Wilhelmshaven, Germany.*

[*]Corresponding author: *dstramski@ucsd.edu*, Tel: (+1) 858.534.3353

Running head: Optical properties of sea-surface microlayer

Keywords: sea-surface microlayer, inherent optical properties, light absorption, light scattering, polarization by scattering, particle concentration, particle size distribution

Declaration of interest: None

Abstract

The sea-surface microlayer (SML) is known to have physical, chemical, and biological properties that are distinctly different from the underlying subsurface water (USW). However, only a few studies in the past reported on measurements of the optical properties of the SML and were limited to light absorption. The light-scattering properties and particle size distribution (PSD), which is one of major determinants of optical variability, have not been previously measured in the SML. In this study we present results for the main inherent optical properties (IOPs), the spectral absorption coefficients and the volume scattering function, as well as particle size distribution, from measurements of the SML and USW in contrasting ocean environments with near-surface chlorophyll-*a* concentration ranging from 0.06 mg m^{-3} in waters off Hawaiian Islands to 1 mg m^{-3} in the Santa Barbara Channel. Our observations also included prominent surface slick conditions associated with a dense bloom of *Trichodesmium*. Significant and highly variable enhancements of the optical properties and particle concentration, including significant changes in the shape of PSD, were observed in the SML compared with USW at all investigated sites. In clear oligotrophic waters the total concentration of particles larger than 0.7 μm in size was enriched in the SML more than 8-fold. In all examined waters the enrichment was consistently higher for larger particles (> 10 μm) than smaller particles. The highest enhancement of light absorption coefficients, > 100-fold for particulate absorption and > 200-fold for phytoplankton absorption in the near-UV and red spectral regions, was observed during the *Trichodesmium* bloom. In clear oligotrophic waters the particulate absorption coefficient was enhanced by as much as 45-fold in the green spectral region and the non-algal component exhibited consistently higher enhancement than phytoplankton component across the examined spectrum. In contrast to absorption, the volume scattering function was enhanced more in clear

oligotrophic waters (> 15-fold at scattering angles ψ between about 65° and 80°) than in the situation of *Trichodesmium* bloom. With the exception of *Trichodesmium* bloom, we consistently observed significantly lower values of the degree of linear polarization of light scattered by suspended particles and whole seawater samples (by as much as 30% in the vicinity of $\psi = 90°$) in the SML compared with USW. This result indicates that the SML can have important effect on the state of polarization of downwelling light entering the ocean and upwelling light leaving the ocean across the air-sea interface. The determinations of IOPs in the SML can extend the capabilities for characterizing constituents of microlayer and provide useful information for radiative transfer and remote-sensing related studies.

1. Introduction

The sea-surface microlayer (SML) is a very thin layer of the ocean which forms the interfacial boundary between the bulk ocean water and atmosphere. Although the thickness of the SML depends on the processes or properties of interest, it has often been defined operationally as the uppermost ocean layer from tens of micrometers to 1 millimeter (Hunter, 1980; Hardy, 1982; Cunliffe et al., 2013; Engel et al., 2017). It has long been recognized that the SML has unique physical (Wangersky, 1976; Soloviev and Lucas, 2014), chemical (Liss, 1975; Hunter, 2005), and biological (Zaitsev, 1971; Cunliffe et al., 2011) properties that are distinctly different from underlying waters. Research conducted over the past decades has greatly advanced an understanding of the complex physicochemical structure and function of the SML and its biological properties. For example, early conceptual models of a "wet-dry" stratified SML (MacIntyre, 1974; Hardy, 1982) have evolved into more complex descriptions implying a major role of gelatinous matter consisting of a complex matrix of various organic macromolecules and gel particles (Sieburth, 1983; Wurl & Holmes, 2008; Cunliffe & Murrell, 2009; Wurl et al. 2011a). Because these materials are sticky and possess strong surface active properties, they facilitate the processes leading to concentration or aggregation of various water constituents within the SML, including microorganisms and other particles. It has been commonly observed that the SML is often significantly enriched in terms of concentration of various dissolved and particulate materials (Carlson, 1983; Cunliffe et al., 2011; Zäncker et al., 2017).

The key aspects of SML composition and its role in various Earth system processes have been summarized in recent reviews (Liss & Duce 2005; Cunliffe et al., 2013; Wurl et al., 2017; Engel et al., 2017). The multi-faceted environmental importance of the SML includes the exchange of momentum, heat and matter (in particular, gases and particles) between the oceans

and atmosphere with impacts on biogeochemical cycling and the Earth's climate, a distinct habitat and food source for a variety of organisms, a unique site for biochemical reactions, and a sink or source of many pollutants. Global relevance of this importance is supported by observations that the presence of the SML is a ubiquitous feature existing under typical oceanic conditions, and thus covering the world's ocean to a significant extent (Wurl et al., 2011b).

The SML also represents a boundary for the transfer of radiant energy into and out of the ocean. To our knowledge, no studies dedicated specifically to the spectral inherent optical properties (IOPs) of the SML, including measurements of both the light absorption and scattering, have as yet been conducted. A few studies have reported measurements of the spectral absorption coefficients of colored dissolved organic matter (CDOM) and suspended particles in microlayer samples in the Atlantic and Pacific Oceans (Obernosterer et al., 2008; Tilstone et al., 2010; Galgani & Engel, 2016; Zäncker et al., 2017). The primary focus of these studies was on enrichment of the microlayer relative to underlying water with microorganisms and various organic constituents, including compounds that play an important role in absorption of ultraviolet (UV) radiation. Significant (more than 2-fold) enhancement of the spectral absorption coefficients of CDOM and phytoplankton was reported in these studies, with some samples exhibiting higher enhancement in the UV compared with the visible portion of the spectrum.

Acquiring quantitative information on the IOPs of the SML can aid in the characterization of SML constituents and propagation of light across the air-sea interface, as well as applications of remote sensing methods to the study of the oceans. In this paper we report on measurements of light absorption and scattering in the SML and underlying subsurface bulk water in contrasting environments in the Pacific Ocean ranging from ultra-oligotrophic waters with near-surface chlorophyll-*a* concentration (Chla) of 0.06 mg m^{-3} to mesotrophic waters with Chla of about 1

mg m^{-3}. We also collected data under prominent surface slick conditions associated with a dense bloom of the cyanobacterium *Trichodesmium*. The optical measurements included the spectral absorption coefficients of CDOM and particulate matter (in some cases partitioned into phytoplankton and non-algal components) with high spectral resolution either within the visible (400–700 nm) or a broader spectral range (300–850 nm). The volume scattering function (VSF) was measured at a single wavelength of 532 nm within a range of scattering angles from less than 1° to ~150°. The degree of linear polarization (DoLP) of scattered light was also determined at scattering angles from about 20° to 150°. In addition, the concentration, composition, and size distribution of suspended particles were measured. Earlier studies indicated that particulate organic matter is consistently enriched in the microlayer, usually to a greater degree than dissolved organic materials (Carlson, 1983; Obernosterer et al., 2008). In our study an emphasis is placed on particulate absorption and scattering properties and characteristics of particulate matter, especially the particle size distribution (PSD). The PSD is one of the major determinants of variability in particle optical properties and, to our knowledge, has not been previously measured in the sea-surface microlayer.

2. Materials and methods

2.1. Study areas

Water samples were collected during two cruises in the Pacific Ocean as part of the Radiance in a Dynamic Ocean (RaDyO) project onboard the *R/V Kilo Moana* (Dickey et al., 2012) The first RaDyO cruise took place in September 2008 in the Santa Barbara Channel, and the second cruise in August–September 2009 in waters off the Hawaiian Islands. General atmospheric and oceanographic conditions during the RaDyO cruises are described in Dickey et al. (2012).

Certain physical and biological features of the RaDyO sampling areas are also summarized in papers devoted to surface-active substances in the SML (Wurl et al., 2009, 2011a).

In this study we present data collected in the Santa Barbara Channel (SBC) at approximately the same location (34° 13′ N, 119° 37′ W, bottom depth of about 170 m) on three consecutive days; 20, 21 and 22 September 2008. From the Hawaiian cruise (HAW) we present data collected on five days; 27 August 2009 (approximate location 19° 15′ N, 156° 10′ W), 28 August 2009 (19° 15′ N, 155° 58′ W), 30 August 2009 (17° 55′ N, 155° 58′ W), 9 September 2009 (17° 37′ N, 158° 17′ W), and 13 September 2009 (17° 51′ N, 159° 22′ W). The sampling area on 27 and 28 August was located in deep water (bottom depth more than 2000 m) relatively close to the west coast of the Island of Hawaii (5–30 km). The three remaining sampling locations were further in the open ocean over 100 km south of the Hawaiian Islands where the bottom depth was about 5000 m. The oceanographic conditions in the selected sampling areas were very different including highly contrasting trophic states ranging from oligotrophic open ocean waters off the Hawaiian Islands to mesotrophic waters in the Santa Barbara Channel and a dense phytoplankton bloom of *Trichodesmium* near the coast of the Island of Hawaii. The water sampling during the *Trichodesmium* bloom (27 Aug 2009) occurred in the presence of a visible surface slick. All the remaining measurements were made under nonslick conditions.

The methodology and instrumentation used for the collection and processing of data presented in this study were similar on the two RaDyO cruises, with some exceptions as described in the following sections.

2.2. Sample collection

The collection of coincident samples from the sea-surface microlayer (SML) and underlying subsurface water (USW) was made from the bow of a small boat operating at a distance of ~500 m from *R/V Kilo Moana* (Wurl et al. 2009, 2011a, 2011b). The SML samples were collected using the glass plate technique by immersing the glass plate vertically into the water and withdrawing it gently (Harvey and Burzell, 1972). The withdrawal rate ranged from about 5 to 6 cm s^{-1} under weak to moderate winds (< 6 m s^{-1}) to 8–10 cm s^{-1} in the presence of larger breaking waves at stronger winds. The thickness of the sampled SML is about 50 μm at slower withdrawal rates and increases to 80–120 μm for faster withdrawal rates (Carlson, 1982; Shinki et al., 2012). We note that the glass plate sampling technique has been reported to be superior for the collection of particles from the SML compared with an alternative screen technique (Estep et al. 1985).

The collection of the SBC samples was made under wind speed ranging from about 1.1 to 9.6 m s^{-1}. The HAW samples were collected at very weak winds less than 2.6 m s^{-1} on two sampling days (27 and 28 Aug 2009) close to the coast of the Island of Hawaii and 4 to 8 m s^{-1} at the open-ocean stations >100 km south of the Hawaiian Islands (30 Aug, 9 Sep, and 13 Sep 2009). The SML samples adhering to the glass plate were scraped off with a neoprene blade and collected in aged polypropylene bottles free of leachable organic matter. The collection of one SML sample (approximately 800 mL) required numerous dips of the glass plate and typically took about 45 min. Concurrent USW samples were collected from a depth of 1 m with a 12-volt DC Teflon gear pump and polypropylene tubing. The USW samples are representative of bulk near-surface water which is typically well mixed in the near-surface layer of the ocean. All comparisons of SML and USW data of particle size distribution, light absorption, and light scattering are based

on USW samples collected at 1 m depth, except for the HAW absorption data from 9 Sep and 13 Sept 2009 when the USW samples were collected at 5 m depth.

Prior to use all sampling equipment was washed with 10% HCl and rinsed with ultrapure de-ionized water. All samples were stored on ice on the small boat until further analysis on board *R/V Kilo Moana*.

2.3. Bulk measures of particle mass concentration and composition

To characterize the bulk particulate assemblages in seawater samples we measured the dry mass concentration of suspended particulate matter (SPM), the concentration of particulate organic carbon (POC), and the concentration of chlorophyll-*a* (Chla). The available volume of SML samples was insufficient to make all these determinations for these samples. As a result, we obtained only a limited amount of POC and Chla data for the SML samples. Similarly, the volume of USW samples from a depth of 1 m obtained during the small boat operation was insufficient for performing consistently all analyses for SPM, POC, and Chla. Therefore, to ensure more complete characterization of subsurface samples, the SPM, POC, and Chla determinations were also made for samples collected at a near-surface depth of about 5 m from a CTD-Rosette equipped with Niskin bottles that were deployed from *R/V Kilo Moana* in close proximity in space and time to small boat operations.

SPM (in units of mg m^{-3}) was determined using a standard gravimetric technique (Van der Linde 1998) after filtration of water samples under low vacuum onto pre-rinsed, pre-combusted glass-fiber GF/F filters (25 mm diameter). The filters were weighed prior to use. Following filtration, sample filters and edges were rinsed with deionized water to remove residual sea salt, dried at 60 °C, and stored sealed until post cruise analysis. The mass of particles collected on the

filters was measured with a Mettler-Toledo MT5 microbalance with 1 μg precision. To determine SPM, the mass of blank filter was subtracted from the mass of sample filter and the result was divided by the filtration volume of the sample.

POC (mg m^{-3}) was determined using a standard method of CHN analysis based on high temperature combustion of sample filters (Parsons et al., 1984; Knap et al., 1996). Water samples were filtered through precombusted 25 mm GF/F filters. The filters were transferred to clean glass vials, dried at 60 °C, and stored until post cruise analysis. Organic carbon content on each sample filter following acidification to remove inorganic carbon was determined with CHN analysis. Similarly, organic carbon content was determined for a number of unused filters to quantify the background carbon content of blank filters. To determine POC, the average value of the blank filters was subtracted from the sample data and the result was divided by the filtration volume of the sample. The concentration of particulate organic nitrogen (PON) was also determined from the CHN analysis.

Samples for Chla (mg m^{-3}) determinations were filtered on 25 mm GF/F filters under low light and then flash frozen and stored in liquid nitrogen until post cruise analysis. The SBC samples were analyzed spectrophotometrically. Acetone extracts of pigments present in the samples were prepared using a 90% acetone solvent. The absorbance spectra of acetone extracts were measured with a dual-beam Lambda 18 spectrophotometer (PerkinElmer, Inc.) equipped with a 15-cm integrating sphere (RSA-PE-18, Labsphere, Inc.). The sample in 1-cm cuvette was placed inside the integrating sphere and measurements were taken within the spectral range from 300 to 850 nm with 1-nm interval. The measured absorbance values at four light wavelengths of 630, 647, 665, and 691 nm (after subtraction of acetone baseline values) were used to calculate Chla from the equation of Ritchie (2008). The HAW samples were analyzed with High

Performance Liquid Chromatography (HPLC) using the analytical procedure described in Ras et al. (2008). In this study we use the HPLC-determined concentration of total chlorophyll-*a* as the measure of Chla, which represents the summed concentrations of mono- and divinyl chlorophyll-*a*, chlorophyllide-*a*, and the allomeric and epimeric forms of chlorophyll-*a*.

Because of limited volume of SML samples, no determinations of SPM were made for the SML samples. On the SBC cruise SPM and Chla were measured for the USW samples (~5 m depth) collected on 20 and 21 Sep 2008. The SPM measurements were made on duplicate samples and averaged. Chla was determined from the analysis of single samples. The filtration volume for these samples was 1 to 1.3 L. POC was measured during the three SBC microlayer experiments (20, 21, and 22 Sep 2008) for both the SML and USW (1 m depth) samples. These determinations were based on single samples with filtration volumes of 400 to 440 mL.

On the HAW cruise SPM was measured for USW samples (1 or 5 m depth) collected on 28 Aug, 9 Sep and 13 Sep 2009 (filtration volume of 4.7 to 6.3L was analyzed). POC and Chla were measured for the SML sample representative of dense *Trichodesmium* bloom (27 Aug 2008, filtration volume of 200 mL) and for USW samples (4.2 to 5.25L) during all HAW experiments.

Differences in the concentrations of various substances between the SML and subsurface water are typically quantified in terms of the enrichment factor, *EF*, which is calculated as a ratio of the concentration in the SML sample to that in the corresponding USW sample. We calculated the *EF* values for POC and Chla for a few cases in which we have data of these parameters for both the SML and USW samples.

2.4. Particle size distribution

The particle size distribution (PSD) was measured for both the SML and USW samples

during all three experiments on the SBC cruise (20, 21, and 22 Sep 2008) and three experiments on the HAW cruise (27, 28, and 30 Aug 2009). These measurements were made on board *R/V* *Kilo Moana* with a Beckman-Coulter Multisizer III using a combination of two aperture sizes, 30 μm and 200 μm. When combined, these measurements spanned the range of equivalent spherical diameter of particles, D, from 0.8 μm (SBC cruise) or 0.7 μm (HAW cruise) to 120 μm. The difference in the lower threshold between the cruises was accepted on the basis of slight differences in the level of instrument noise. Both apertures were calibrated using NIST-traceable microsphere standards of known size. The Coulter technique and potential sources of uncertainties in particle counting and sizing with this technique are described in detail in Jonasz & Fournier (2007).

Each discrete Coulter measurement consisted of a set of values representing the number of particles per unit volume of water within a size class, $N(D)$ (in units of m^{-3}). The 0.2 μm filtered seawater was used as the blank and subtracted from particle counts of the sample. Multiple replicate measurements of the PSD (usually > 10 and as many as 22 with the 30 μm aperture and 27 with the 200 μm aperture) were taken for each sample and summed to provide larger sample volumes and improved statistical accuracy of particle counts. Total sample volumes after the summation of replicate measurements averaged about 2.1 mL (range 0.7–5 mL) for the 30 μm aperture and 130 mL (range 22–228 mL) for the 200 μm aperture.

The Coulter technique yields high-resolution measurements of size on individual particles. For each aperture, the data were acquired using 256 size bins logarithmically spaced over the measured range. The width of individual size bins, ΔD, is dependent upon the aperture size and diameter of the size class. For example, ΔD ranges from as little as 0.01 μm for the 30 μm aperture to as large as 1.6 μm for the 200 μm aperture. To create the final distribution,

measurements from both apertures were merged at an overlapping size class (D ~ 5.1 μm for the SBC data and ~4.8 μm for the HAW data) which shared a similar midpoint of the bin and bin width. Because the total particle counts from replicate measurements for large particles ($D \gtrsim 20$ μm) were often small (< 10) in the original size bins, the PSDs in this size range exhibited significant bin-to-bin variations. To reduce this problem the particle counts in this size range were rebinned using broader size bins. As a result we obtained improved particle counts per bin (> 50) extending to about 50 μm with the last bin between about 40 μm and 49 μm. The PSD data beyond 50 μm are not reported because of inadequate statistics associated with low particle counts.

The density function of the particle number distribution, $F_N(D)$ (m^{-3} μm^{-1}), was calculated by normalizing the concentration of particles within each size bin, $N(D)$, to the bin width, ΔD (in units of μm) (Jonasz & Fournier, 2007). The particle volume distribution was calculated as $V(D) = N(D)\ \pi D^3/6$, where D represents here a mid-point diameter of the size bins and $V(D)$ is dimensionless as $N(D)$ and D can be expressed in the same units of length. The density function of the particle volume distribution, $F_V(D)$ (μm^{-1}), was calculated by normalizing $V(D)$ to ΔD. For comparing the PSDs in the SML and USW samples the size dependent enrichment factor, EF, was calculated as a ratio of $F_N(D)$ [or equivalently $N(D)$] for the SML sample to $F_N(D)$ [or $N(D)$] for the corresponding USW sample. We note that this enrichment factor based on particle number concentration is identical to that calculated on the basis of particle volume distribution.

2.5. Light absorption measurements

Discrete samples of the SML and USW were also used for optical measurements of the absorption coefficient and the volume scattering function. These two optical quantities represent

the fundamental inherent optical properties (IOPs) of seawater (Mobley, 1994). On the SBC cruise the spectral absorption coefficients (in units of m^{-1}) of colored dissolved organic matter (CDOM), $a_g(\lambda)$, and suspended particulate matter, $a_p(\lambda)$, were measured within the spectral range 400–700 nm on board *R/V Kilo Moana* using a point-source integrating-cavity absorption meter (PSICAM; Röttgers & Doerffer, 2007; Röttgers et al. 2007). The sample volume of about 400 mL was required for PSICAM measurements. First, the light absorption spectra of SML and USW samples were measured, from which the baseline measurements of freshly purified water were subtracted to obtain the spectral absorption coefficient of the sum of particulate and dissolved matter, $a_{pg}(\lambda)$. The sample was then filtered through a purified water-washed and sample-washed 0.2-µm membrane filter (GSWP, Millipore) and the filtrate was measured to determine the CDOM component, $a_g(\lambda)$. The particulate component, $a_p(\lambda)$,was determined as a difference between $a_{pg}(\lambda)$ and $a_g(\lambda)$. The calculations of the absorption coefficients and corrections for temperature, salinity, and chlorophyll fluorescence effects were done as described in Röttgers et al. (2007). The PSICAM was calibrated daily using a nigrosin (Merck) dye solution whose absorption coefficient was determined using a liquid waveguide capillary cell (LWCC, WPI Inc, U.S.A). The LWCC setup consisted of a capillary cell (LWCC-2200, WPI, U.S.A., pathlength 200 cm), a UV/VIS spectrometer (USB4000, OceanOptics, U.S.A) and a UV/VIS fiber optic light source (DH2000S, OceanOptics, U.S.A.). The three components are optically connected using two fiber optics. Collections of light spectra are made using the SpectraSuite software (OceanOptics, U.S.A.). These measurements were made as described in Lefering et al. (2017), using purified water as a reference and a 100g/L NaCl solution to determine the salinity correction coefficient for the LWCC setup. All measurements were done in triplicates and averaged.

On the HAW cruise the samples were prepared on board *R/V Kilo Moana* for post cruise measurements of the spectral absorption coefficient of particles, $a_p(\lambda)$, with a filter-pad technique (Bricaud & Stramski, 1990; Mitchell, 1990; Röttgers & Gehnke, 2012; Stramski et al., 2015). Specifically, the particulate matter was collected by filtration of the SML and USW (1 m depth) samples onto 25 mm GF/F filters during all five microlayer experiments (27, 28, 30 Aug, and 9 and 13 Sep 2009). The filtration volume ranged from 200 to 600 mL for the SML samples and 4.2 to 4.75 L for the USW samples. The samples were flash frozen and stored in liquid nitrogen until post cruise analysis. The measurements of $a_p(\lambda)$ were made at 1 nm intervals over the spectral range 300–850 nm with a dual-beam Lambda 18 spectrophotometer (Perkin Elmer, Inc.) equipped with a 15 cm integrating sphere (RSA-PE-18, Labsphere, Inc.). Sample filters were placed inside the integrating sphere for measurement (Röttgers & Gehnke, 2012; Stramski et al., 2015). Duplicate spectral scans were taken for two different orientations of the sample filter and the results were averaged. The agreement between the two scans was very good (within a few percent). Similar measurements were taken for several blank filters. The average spectrum of the blank filters was subtracted from the sample spectra to yield the baseline-corrected data. A correction for the pathlength amplification factor that was developed for a specific configuration of the filter-pad technique with filters placed inside the integrating sphere was applied to yield the final data of $a_p(\lambda)$ following the recommendation in Stramski et al. (2015).

On the HAW cruise, additional absorption measurements were made on the sample filters following pigment extraction with methanol in order to partition $a_p(\lambda)$ into the contributions of phytoplankton, $a_{ph}(\lambda)$, and non-algal, $a_{NAP}(\lambda)$, components (Kishino et al., 1985). As for $a_p(\lambda)$ the same correction for pathlength amplification was applied to measurements of $a_{NAP}(\lambda)$. The values of measured $a_{NAP}(\lambda)$ were very close to $a_p(\lambda)$ in the near-infrared (near-IR) spectral region (800–

850 nm) supporting negligible absorption by phytoplankton at these wavelengths. To satisfy the assumptions that $a_{ph}(\lambda) = 0$ and $a_p(\lambda) = a_{NAP}(\lambda)$ in the near-IR even more closely, the final data of $a_{NAP}(\lambda)$ were slightly adjusted by adding the average value of the difference between the measured $a_p(\lambda)$ and the measured $a_{NAP}(\lambda)$ in the spectral region 800–850 nm to the measured values of $a_{NAP}(\lambda)$. The final data of $a_{ph}(\lambda)$ were then obtained as a difference between $a_p(\lambda)$ and $a_{NAP}(\lambda)$. These results should be used with caution because methanol extraction has some limitations, for example this method does not remove water soluble phycobilipigments and occasionally results in incomplete extraction of pigments.

For a few HAW samples (27 Aug and 13 Sep 2009) the measurement of $a_p(\lambda)$ was also partitioned into $a_{NAP}(\lambda)$ and $a_{ph}(\lambda)$ with a bleaching method of Ferrari and Tassan (1999). Bleaching was conducted by exposing the sample filter to a few drops of 1:10 (volume:volume) diluted bleach (NaOCl, 1% active Cl) for a few minutes before taking a spectrophotometric measurement of $a_{NAP}(\lambda)$. In this method pigments are oxidized but remain within the particulate matter on the filter. These results of absorption partitioning should be also used with caution owing to methodological limitations, especially inaccuracies in the short-wavelength portion of the visible spectrum and UV. We also note that both the PSICAM technique used during the SBC experiment and the filer-pad technique with an inside integrating sphere configuration used during the HAW experiment are currently considered the best methods for measuring the particulate absorption coefficient (Röttgers, 2018; Roesler et al., 2018).

2.6. Light scattering measurements

Measurements of the volume scattering function (VSF) of seawater samples, denoted as $\beta(\psi)$ (in units of m^{-1} sr^{-1}), were made with two instruments, a Laser In Situ Scattering and

Transmissometry (LISST-100X type B, Sequoia Scientific Inc., hereafter referred to as LISST) and a DAWN-EOS (Wyatt Technology Corp., hereafter referred to as DAWN). Both instruments were used to measure VSF for the SML and USW samples during the SBC cruise. On the HAW cruise only the DAWN instrument was used and these measurements were made during three experiments (27, 28 and 30 Aug 2009). Both instruments provide multi-angle measurements of VSF at the same light wavelength λ = 532 nm. The LISST is equipped with a semiconductor laser diode system (ChromaLase, Blue Sky Research, Inc.) producing a linearly polarized beam of light of about 10 mm in diameter. The DAWN uses a diode-pumped frequency-doubled Nd-YAG laser with a beam of 62 μm in diameter. The DAWN measurements are conducted with the linearly polarized incident beam either with perpendicular (vertical) or parallel (horizontal) polarization relative to the scattering plane. This plane is defined to contain the incident and scattered beams. The range of scattering angle ψ covered by the two instruments is different. The LISST uses 32 ring detectors providing measurements of forward light scattering at 32 angles over the approximate range from 0.08° to 13.5° (Agrawal & Pottsmith, 2000). The DAWN uses 18 photodiode detectors providing measurements at 18 angles over the range 22.5° to 147° (Babin at al., 2012). The LISST and DAWN detectors measure scattered light without polarization analyzers and are assumed to be insensitive to polarization.

As the measurements were performed in the bench-top mode of operation, the LISST was equipped with a sample chamber inserted into the optical head of the instrument. The space surrounding the optical path was covered with a dark cloth to prevent stray light effects associated with ambient light (Reynolds et al., 2010; Andrews et al., 2011). The path length of the illuminated sample was 5 cm. For a given sample, the measurement consisted of acquisition of time series data taken at 1 Hz sampling frequency. Two to four time series, each ranging from

about 10 to 20 min in duration, were acquired for each sample on the SBC cruise. The cumulative duration of the acquisition of time series data for different samples ranged from about 20 to 55 min, so that the total number of repeated scans of VSF ranged from about 1200 to 3300. For each sample, these repeated scans were averaged to yield the mean values of VSF. Similar measurements were collected on 0.2-μm (Millipore membrane) filtered seawater to determine the mean baseline values representative of pure seawater. These baseline measurements were subtracted from the mean sample measurements to yield the final LISST data of particulate volume scattering function, $\beta_p(\psi)$. We note that the manufacturer's calibration of LISST was based on a nominal radiant sensitivity of ring detectors (amperes of photoelectric current per watt of optical power) traceable to the National Institute of Standards and Technology (Agrawal, 2005; Agrawal & Mikkelsen, 2009). It is also important to recall that the VSF is defined for the total intensity of scattered light measured without polarization analyzer when the sample is illuminated by randomly polarized (unpolarized) incident beam. This definition links the VSF to the first element, M_{11}, of a 4 x 4 scattering matrix also referred to as Mueller matrix (Jonasz & Fournier, 2007). The potential errors introduced to the LISST-derived $\beta_p(\psi)$ as a result of using a linearly polarized incident beam are very small within the forward angular range of LISST measurements ($\psi < 13.5°$) for natural assemblages of marine particles (Slade & Boss, 2006). We also note that for all SBC samples examined in this study the $\beta_p(\psi)$ values within the range of forward scattering angles of LISST are approximately (to within less than 0.5%) equal to the total volume scattering function of seawater, $\beta(\psi)$, which includes both the particulate and molecular scattering contributions.

The DAWN measurements were made with a sample placed in a 20 mL cylindrical glass vial. The interrogated sample volume was on the order of 10 nL. The DAWN measurements using

such configuration have been previously characterized and calibrated (Babin et al., 2012). The calibration of DAWN was based on measurements of light scattered at 90^{o} by pure toluene with the incident beam having a linear perpendicular polarization. This calibration relies on known magnitude of molecular scattering by toluene. To encompass the large dynamic range of scattered intensity, three selectable gain settings are available for each DAWN detector (gain factors of 1, 21, or 101). In our experiments the gain settings were adjusted separately for each detector to avoid potential saturation of the measured signal.

The small sample volume required for DAWN measurements can be considered as an advantage for microlayer experiments because the available volume of SML samples is typically limited. However, the small volume of illuminated sample also implies some limitations of DAWN in terms of adequately resolving the presence of relatively large particles in seawater. Previous test measurements of particles as large as 20 μm in diameter (standard spherical polystyrene beads) yielded generally satisfactory results as indicated by comparisons with theoretical Mie scattering predictions but similar assessments for larger-sized particles were not made (Babin et al., 2012). In general, the DAWN measurements of natural seawater samples should be viewed with due caution with regard to the effects of large particles, especially because there is potential for underestimating the contribution of large particles to light scattering. However, as large particles occur in seawater typically at very low concentrations compared to smaller particles (Bader, 1970; Jonasz & Fournier 2007), this potential underestimation is expected to be important only for samples in which large particles are relatively more abundant. We note that this potential effect was not evident in earlier tests of DAWN with several seawater samples collected in the near-shore zone at Scripps Institution of Oceanography in La Jolla (Babin et al., 2012). The limitation associated with small sampling

volume of DAWN can be also mitigated to large extent by the expected dominant contribution of relatively small particles (less than about 10 μm) to light scattering in typical open ocean conditions (Morel & Ahn, 1991; Stramski & Kiefer, 1991).

The DAWN instrument was equipped with a liquid crystal variable retarder (LRC-100-VIS, Meadowlark Optics) to produce incident light with two linear polarization states; horizontal and vertical relative to the scattering plane. During the process of setting the retarder to produce the beam with linear polarizations, we measured the contrast (or extinction) ratio of the linear polarization for both the vertical and horizontal polarization settings of the retarder. This value, representing the ratio of the maximum to minimum light intensity of the two linearly polarized components transmitted for a given polarization setting of the retarder, was close to or higher than 700:1 and was similar (within 5%) for both polarization settings of the retarder.

We here define the measured intensity of scattered light, $I_H(\psi)$, for the horizontal polarization of the incident beam and the measured intensity of scattered light, $I_V(\psi)$, for the vertical polarization of the incident beam. For each SML and USW sample collected on the SBC and HAW cruises, replicate measurements were taken and averaged for each polarization state of the incident beam. Specifically, for a given sample, the data acquisition protocol consisted of collecting time series measurements of $I_H(\psi)$ and $I_V(\psi)$ with sampling frequency of 8 Hz. Typical duration of time series measurement for each polarization state was 3 minutes which provided 1440 data points. Such sets of time series measurements were repeated six to nine times and each of these replications was made with a different randomly chosen orientation of sample vial within the instrument. The sample was gently mixed between these replicate measurements. For a specific orientation of sample vial the measurements of $I_H(\psi)$ and $I_V(\psi)$ were averaged to represent that orientation. Such results were then averaged for all replicate measurements taken

with different vial orientations to yield the final values of $I_H(\psi)$ and $I_V(\psi)$. Depending on the number of replicate measurements, the total number of data points involved in the calculation of final averages of $I_H(\psi)$ and $I_V(\psi)$ ranged from 8640 to 12960 for different samples analyzed in our experiments.

The measurements of $I_H(\psi)$ and $I_V(\psi)$ allow for the determinations of the $M_{11}(\psi)$ and $M_{12}(\psi)$ elements of the scattering matrix; specifically the measurement of $I_H(\psi)$ provides the sum $M_{11}(\psi) + M_{12}(\psi)$ and the measurement of $I_V(\psi)$ the difference $M_{11}(\psi) - M_{12}(\psi)$ (Bohren & Huffman, 1983; Bickel & Bailey, 1985). As the volume scattering function $\beta(\psi)$ is directly linked to $M_{11}(\psi)$, it can be derived from $[I_H(\psi) + I_V(\psi)]/2$ and expressed in units of (m^{-1} sr^{-1}) using the calibration procedure described in Babin et al. (2012). The $M_{12}(\psi)$ can be derived from $[I_H(\psi) - I_V(\psi)]/2$. Previous measurements of scattering matrix for oceanic waters indicated that all non-diagonal elements of scattering matrix, except $M_{12}(\psi)$ and $M_{21}(\psi)$, are zero to within the experimental error (Voss & Fry, 1984). These measurements also indicated that $M_{12}(\psi)$ is approximately equal to $M_{21}(\psi)$. For scattering media exhibiting such properties the degree of linear polarization (DoLP) of scattered light by the sample illuminated by unpolarized beam is defined as $P(\psi) = -M_{12}(\psi)/M_{11}(\psi) = [I_V(\psi) - I_H(\psi)]/[I_V(\psi) + I_H(\psi)]$ where positive values of $P(\psi)$ are for dominantly vertical polarization and negative values for dominantly horizontal polarization (Volten et al., 1998; Hovenier et al., 2002; Kokhanovsky, 2003). For all SML and USW samples measured in this study with DAWN, $P(\psi)$ was determined from $[I_V(\psi) - I_H(\psi)]/[I_V(\psi) + I_H(\psi)]$. We note that this definition of DoLP has been widely used for characterizing the inherent scattering properties of various types of aquatic particles, aerosol

particles, and cosmic dust (Volten et al., 1998, 2001; Petrova et al., 2000). We also note that this inherent DoLP of light scattered by particles suspended in seawater (or the entire seawater sample including contributions of water molecules and particles) should not be confused with the degree of linear polarization of ambient radiance field in the ocean, which has been commonly reported in oceanographic literature (e.g., Waterman, 1954; Ivanoff, 1974; Adams et al., 2002; Gilerson et al., 2013; Ibrahim et al., 2016).

The DAWN measurements yielded the $\beta(\psi)$ and $P(\psi)$ values representing seawater samples with combined contributions of particulate and molecular scattering. Within the angular range of DAWN the molecular component of scattering can be significant, so the particulate component of VSF, $\beta_p(\psi)$, was obtained by subtracting the pure seawater component, $\beta_w(\psi)$, from the total $\beta(\psi)$. The $\beta_w(\psi)$ values at 532 nm were calculated from the model of water molecular scattering (Zhang et al., 2009) using the measured temperature (T) and salinity (S) of underlying subsurface water samples and a constant depolarization ratio, $\delta = 0.039$, for water molecules. For the SBC samples T = 18 °C and S = 33.5 PSU. For the HAW samples T ranged from 26.4 to 27.1 °C and S was 35 to 35.1 PSU. The particulate component of DoLP, $P_p(\psi)$, was also obtained by accounting for the contribution of seawater molecules to total $P(\psi)$. Specifically, $P_p(\psi)$ was calculated from the expression in which $P(\psi)$ is written as the weighted sum $P_w(\psi)$ $[\beta_w(\psi)/\beta(\psi)]$ + $P_p(\psi)$ $[(\beta_p(\psi)/\beta(\psi)]$, where $P_w(\psi)$ is the DoLP of light scattered by seawater molecules and $\beta(\psi) = \beta_w(\psi) + \beta_p(\psi)$ (Morel, 1973). The $P_w(\psi)$ values were obtained from calculations of vertically and horizontally polarized light scattered by molecules using the same values of T, S, and δ as above (Zhang et al., 2019). The calculated values of $P_w(\psi)$ are actually independent of T and S because of the assumed constancy of δ. From these calculations the maximum value $P_{w,max}$ occurs at $\psi = 90°$ and is about 0.92, which is higher than earlier estimates (Morel, 1973).

For each optical property determined in this study, we calculated a ratio of the values for the SML sample to the values for the corresponding USW sample. This ratio is referred to as the enhancement factor and is denoted by the same symbol *EF* as the enrichment factor.

3. Results and discussion

3.1. Concentration, composition, and size characteristics of suspended particles

The particle concentration characteristics of near-surface water varied greatly among the investigated sites. At the near-surface depths of 1 to 5 m, Chla, POC, and SPM varied respectively from about 0.057, 34, and 92 mg m^{-3} in open ocean waters off the Hawaiian Islands to 1, 290, and 555 mg m^{-3} in the Santa Barbara Channel (Table 1). The total number concentration of particles within the size range measured with the Coulter technique (i.e., > 0.8 μm for the SBC samples and > 0.7 μm for the HAW samples) was also significantly lower in the USW samples from the HAW cruise than the SBC cruise (Table 1). The values of the POC/SPM ratio varied, however, within the same range from 0.36 to 0.52 in both investigated regions. The POC/SPM ratio provides a useful proxy for the composition of particulate matter in terms of organic and inorganic fractions (Woźniak et al., 2010) and our measurements indicate that organic particles dominated the suspended particulate matter in all USW samples. However, we have no information on the potential differences in POC/SPM between the SML and USW because no SPM measurements were made in the SML.

In the Santa Barbara Channel the SML was markedly enriched in POC by factors within the range 1.6 to 2.6 (Table 1), consistent with earlier data from coastal Mediterranean waters sheltered from pollution and terrestrial sources (Daumas et al., 1976). A broader range of POC enrichment (1.3 to 7.6) was previously observed in oligotrophic waters of the South Pacific

Ocean (Obernosterer et al., 2008). We also note that in the SBC we observed higher POC/PON ratios (by 35–60%) in the SML compared with USW, consistent with observations of Obernosterer et al. (2008). On the HAW cruise we made only one measurement of POC enrichment in the SML, which was 23 (Table 1). This very high value was observed under extreme conditions during a dense bloom of *Trichodesmium* in the presence of a visible surface slick (27 August 2009) when POC increased from 96 mg m^{-3} in the USW to 2250 mg m^{-3} in the SML. Under these conditions we also observed a dramatic increase in Chla from 0.065 mg m^{-3} in the USW to 15.37 mg m^{-3} in the SML. This change yields a very high Chla enrichment of 236 (Table 1), which appears to be the highest reported in literature.

Previous measurements of Chla under nonslick conditions indicated variable *EF* but typically significantly below 10 (Daumas et al., 1976; Joux et al., 2006; Tilstone et al., 2010) and in some cases a Chla depletion in the SML (Obernosterer et al., 2008). The Chla enrichment higher than 10 was, however, reported for slick conditions (Hardy & Apts, 1989; Tilstone et al., 2010). To our knowledge, the previously reported maximum of *EF* for Chla is about 63, which was observed in the Atlantic Ocean in the presence of a visible surface slick and high concentration of dinoflagellates *Prorocentrum* spp. (Tilstone et al., 2010). Although the determinations of *EF* for various water constituents depend on the method of SML sampling and a reference depth of USW (Agogué et al., 2004; Tilstone et al., 2010), our data obtained during *Trichodesmium* bloom provide an indication of the scale of the potential enrichment of Chla and POC in the SML.

Particle size distributions (PSDs) measured on the SML and USW samples in the Santa Barbara Channel and off the Hawaiian Islands are illustrated in Figs. 1 and 2 respectively. Data from two experiments from each cruise are depicted. The particle number distributions, $F_N(D)$,

show a characteristic rapid decrease of particle concentration with increasing particle diameter (Fig. 1a,b and Fig. 2a,b). For all SML samples these distributions show significant changes in slope across the examined size range with the presence of significant peaks corresponding to increased concentrations of particles within specific size ranges. These features are particularly well-pronounced in the distributions of particle volume concentration (Fig. 1b,d and Fig. 2b,d). In the Santa Barbara Channel the distributions of the USW samples also show distinct features (Fig. 1), which emphasizes the difficulty in characterizing $F_N(D)$ with a power function consisting of a single slope value (Reynolds et al., 2010). In waters off the Hawaiian Islands, however, the PSD of the USW samples is generally featureless with an overall slope of the $F_N(D)$ distribution being consistent with a slope of −4 across the size range (Fig. 2). Most importantly, Figures 1 and 2 show consistently higher magnitude of PSD for all SML samples compared with the corresponding USW samples across the entire examined size range and also considerable differences in the PSD shape between the SML and USW. This result indicates that whereas the enrichment of particle concentration in the microlayer occurs at all examined sizes, the magnitude of enrichment is dependent on particle size.

The observed large differences in both the magnitude and shape of the PSD between the SML and USW samples suggest strong potential for differences in the optical properties of these two particle assemblages. This potential is characterized by the data of the enrichment factor (*EF*) for PSD in the surface microlayer (Fig. 3). We note that these data are equally applicable to the particle number concentration, particle volume concentration, or particle area concentration; albeit the latter type of size distribution is not presented explicitly in this paper. The *EF* values are generally smaller in the mesotrophic waters of the Santa Barbara Channel (Fig. 3a) than those observed in waters offshore of the Hawaiian Islands (Fig. 3b). The enrichment of the total

particle concentration integrated over the entire examined size range varied from 1.3 to 2.2 for the SBC samples and from 3 to 8.7 for the HAW samples (Table 1) with the highest value for the sample representing the open ocean oligotrophic waters (Fig. 3b, solid gray line).

All our data of *EF* as a function of particle diameter have a characteristic pattern indicating higher enrichment of particles larger than about 10 μm compared with smaller particles. In the Santa Barbara Channel the highest *EF* values in the range 6 to 7 were observed in the size range between about 12 μm and 18 μm (Fig. 3a, solid black line). In the open ocean oligotrophic waters off the Hawaiian Islands the *EF* values were very high in the range 30 to 40 for particle diameters between 10 μm and 20 μm, and even higher of 40 to 70 between 20 μm and 30 μm (Fig. 3b, solid gray line). In this case the enrichment also exhibited a conspicuous secondary maximum with the *EF* values varying between 10 and 15 for small particles in the diameter range from about 1 μm to 6 μm. Under exceptional surface slick conditions during a dense bloom of *Trichodesmium* the *EF* also reached relatively high values of 20 to 30 in the diameter range 10 μm to 20 μm (Fig. 3b, solid black line). In this case, however, our data indicate a further strong increase of *EF* up to about 100 for large particles of 30 μm to 50 μm. Although the statistics based on particle counts is poorest for these large particles this trend of strong increase of *EF* appears realistic owing to the appropriate rebinning of size data as described in Section 2.4. Thus, among our observations, the *Trichodesmium* bloom data show by far the strongest size dependency of particle concentration enrichment with the *EF* values varying from less than 4 for small particles < 2 μm to more than 50 for large particles > 30 μm.

3.2. Spectral absorption coefficients

In the Santa Barbara Channel both the SML and USW samples were generally characterized

by lower values of $a_g(\lambda)$ than $a_p(\lambda)$ throughout the visible spectrum with the exception of short-wavelength end of the spectrum, especially for USW samples. For example, at 440 nm the range of the a_g/a_p ratio for the three USW samples was 0.59 to 0.68. This ratio was more variable in the SML with a range of 0.12 to 0.57. The magnitudes of $a_g(440)$ and $a_p(440)$ in the USW varied from 0.04 to 0.048 m^{-1} and 0.058 to 0.076 m^{-1}, respectively. In the SML the range of variability was 0.049 to 0.055 m^{-1} and 0.087 to 0.199 m^{-1}, respectively. Example absorption spectra of $a_g(\lambda)$ and $a_p(\lambda)$ measured on the SML and USW samples in the SBC are depicted in Fig. 4. These measurements indicate higher absorption coefficients in the SML than USW with much more pronounced differences between the SML and USW for $a_p(\lambda)$ than $a_g(\lambda)$. The $a_p(\lambda)$ spectrum of the USW has well-pronounced features of phytoplankton absorption. These features are also present in the SML although they are somewhat weaker in the blue spectral region owing to an apparent increase of the contribution by non-algal particles. The significant role of non-algal particles in the SML is also supported by substantial absorption at the long-wavelength end of the spectrum at 700 nm.

For the five USW samples examined during the HAW cruise, the magnitude of $a_p(\lambda)$ and the proportions of $a_{ph}(\lambda)$ and $a_{NAP}(\lambda)$ remained within a relatively narrow range of variation. For example, $a_p(440)$ varied from 0.007 m^{-1} (30 Aug 2009) to 0.0097 m^{-1} (28 Aug 2007). These USW values are considerably lower than those observed in the SBC, which is consistent with measurements of SPM, POC, and Chla during both cruises. It is also important to note that $a_p(440)$ of the USW was 0.0095 m^{-1} for the slick conditions in the presence of dense *Trichodesmium* bloom (27 Aug 2009), which remains within the range of relatively low values observed during the HAW cruise. For the USW samples the variability in the contributions of $a_{ph}(\lambda)$ and $a_{NAP}(\lambda)$ to total particulate absorption was also quite constrained. For example, the

$a_{ph}(440)/a_p(440)$ ratio varied from 0.73 (9 Sep 2009) to 0.8 (13 Sep 2009), indicating the dominant role of phytoplankton in the near-surface particulate absorption within the region of HAW cruise.

In contrast to the USW, $a_p(\lambda)$ exhibited much larger variation for the SML samples from the HAW cruise. The lowest values of $a_p(440)$ in the range 0.022 to 0.025 m^{-1} were measured at open ocean stations (9 and 13 Sep 2009). The highest value of 0.484 m^{-1} was measured under slick conditions in the presence of *Trichodesmium* bloom (27 Aug 2009), which reflects a very high enhancement of particulate absorption in the SML compared to USW. The range of the ratio $a_{ph}(\lambda)/a_p(\lambda)$ was also much larger in the SML than USW. The $a_{ph}(440)/a_p(440)$ ratio varied from 0.34 (28 Aug and 13 Sep 2009) to 0.85 (27 Aug 2009). The only SML sample that showed the dominant contribution of $a_{ph}(440)$ to $a_p(440)$ was that collected during the *Trichodesmium* bloom in the presence of surface slick (27 Aug 2009). The value of $a_{ph}(440)/a_p(440)$ for the four remaining SML samples was less than 0.5, indicating a dominant role of non-algal particulate absorption. Thus, in the absence of extreme events such as *Trichodesmium* bloom, our data from oligotrophic waters off the Hawaiian Islands suggest that whereas the particulate absorption in the near-surface bulk seawater is dominated by phytoplankton, the SML particulate absorption is dominated by non-algal particles. This result points to preferential selectivity for concentrating and maintaining non-algal particles within the SML in open ocean environments regardless of whether the particles originate from the underlying water column or atmospheric deposition.

Figure 5 shows example spectra of $a_p(\lambda)$, $a_{NAP}(\lambda)$, and $a_{ph}(\lambda)$ measured on the HAW cruise. The event of dense *Trichodesmium* bloom is illustrated in Fig. 5a,b,c, which shows strong phytoplankton absorption features in the $a_p(\lambda)$ spectra for both the SML and USW samples, the dominance of $a_{ph}(\lambda)$ over $a_{NAP}(\lambda)$ for both the SML and USW samples, and a very high

enhancement of the absorption coefficients in the SML compared with USW. The insets in Fig. 5a,c show an absorption feature in the UV which is most likely associated with very high concentration of mycosporine-like amino acids (MAAs) in *Trichodesmium*, especially in the SML. We note, however, that the data in the UV, especially at wavelengths shorter than 350 nm, should be viewed with caution, especially in quantitative sense, because of increased uncertainties of particulate absorption obtained with the filter-pad technique in the UV (Stramski et al., 2015). We also note that significant enhancement of UV absorption in the SML associated with MAAs has been demonstrated and discussed in earlier studies (Tilstone et al., 2010).

Figure 5b also shows the differences in $a_{NAP}(\lambda)$ for the SML sample obtained with two partitioning methods. The result obtained with the methanol extraction exhibits maxima in the $a_{NAP}(\lambda)$spectrum which can be attributed to non-extracted phycobilipigments and possibly also incomplete extraction of other pigments as indicted by residual maximum in the red band of chlorophyll-*a*. The result obtained with the NaOCl bleaching method exhibits featureless spectrum of $a_{NAP}(\lambda)$ with lower values compared to the methanol method within the visible spectrum. However, because of the dominant role of phytoplankton absorption in this sample, the effect of these differences in $a_{NAP}(\lambda)$ on the determination of $a_{ph}(\lambda)$ is small, e.g., only about 6% at 440 nm (Fig. 5c).

The absorption spectra collected in clear oligotrophic waters off the Hawaiian Islands also show significant enhancement in the SML compared with USW (Fig. 5d,e,f). Another important result is that while phytoplankton absorption maxima in the visible spectral region are clearly evident in the USW spectra of $a_p(\lambda)$, such features are not readily detectable in the SML data that have the spectral shape typical for particulate assemblages dominated by non-algal particles (Fig. 5d,e). For the samples illustrated in Fig. 5d,e,f the $a_{ph}(440)/a_p(440)$ ratio decreased from 0.77 in

630 the USW to 0.35 in the SML sample. In the SML, even $a_{ph}(\lambda)$ does not show clear absorption maxima in the visible spectrum but is dominated by the UV absorption, most likely associated with a photoprotective function (Fig. 5f).

An important feature of the $a_p(\lambda)$ and $a_{NAP}(\lambda)$ spectra in clear oligotrophic waters off the Hawaiian Islands is significant absorption in the near-IR part of the spectrum for the SML
635 sample, which is much larger compared with very small or negligible near-IR absorption for the USW sample (Fig. 5d,e). This result is also consistent with our $a_p(\lambda)$ data at the long-wavelength end of the visible spectrum from the mesotrophic waters of the Santa Barbara Channel (Fig. 4b). Such high absorption in the near-IR in the SML can be indicative of specific particle types or of their origin. Particles in the SML can originate from the underlying water column and deposition
640 from the atmosphere. The organic particles present in the water column, both living and non-living, are expected to have very low or negligible absorption in the near-IR (Babin & Stramski, 2002). However, it was also previously demonstrated that various samples of mineral-rich particulate assemblages suspended in water can exhibit significant absorption in the near-IR, especially when iron-bearing particles are present in the samples (Babin & Stramski, 2004;
645 Stramski et al., 2007). In the atmospheric literature, iron oxides associated typically with mineral dust have been also recognized as an important absorbing component of the atmospheric particulate matter in the visible spectrum but the graphitic form of carbon (often referred to as black carbon or light-absorbing carbon) has been thought to be by far the dominant absorbing component in the visible and near-IR (Lindberg, 1975; Lindberg et al., 1993; Arimoto et al.,
650 2002; Schuster et al., 2005; Bond & Bergstrom, 2006). Although we cannot discriminate between the different sources of the SML particles investigated in our study, it is conceivable that atmospheric deposition may have an important or perhaps even the dominant role as a

source of absorbing non-algal particles in the SML. Circumstantial evidence supporting this possibility is provided by earlier measurements of significant near-IR absorption of various atmospheric dust samples suspended in water and estimates of sizable effect of atmospheric deposition on the optical properties of surface ocean waters (Stramski et al., 2004, 2007; Stramska et al., 2008).

The enhancement of light absorption in the SML is illustrated with data from the SBC and HAW cruises in Figs. 6 and 7 respectively. The SBC data show higher values of the enhancement factor (*EF*) for particulate absorption than CDOM absorption (Fig. 6a,b). The *EF* values for $a_g(\lambda)$ were as high as about 1.25 in the blue spectral region. For $a_p(\lambda)$ the *EF* values were as high as 2.5 in the blue and reached or exceeded 6 between 560 nm and 600 nm. In the blue and green spectral regions where $a_g(\lambda)$ is significant the spectral dependence of *EF* for CDOM absorption is relatively weak (Fig. 6a). In the red spectral region $a_g(\lambda)$ is very low, so the interpretation of the magnitude and spectral behavior of *EF* in this region is limited. In contrast to $a_g(\lambda)$, the *EF* for particulate absorption exhibits much stronger dependence on light wavelength with spectral minima coinciding approximately with the blue and red bands of phytoplankton absorption. Because $a_p(\lambda)$ is enhanced more than $a_g(\lambda)$, the *EF* for the sum $a_g(\lambda) + a_p(\lambda)$ has a similar spectral pattern to that for $a_p(\lambda)$ albeit the magnitude is lower (Fig. 6c). The spectral behavior of *EF* for total absorption coefficient, $a(\lambda)$, is characterized by the highest values in the blue (> 2 at $\lambda < 425$ nm) and the lowest values (< 1.1) in the long-wavelength end of visible spectrum (Fig. 6d). These low values in the red are attributable to dominant contribution of molecular water absorption in this spectral region. For calculating $a(\lambda)$ we used the values of pure water absorption coefficient, $a_w(\lambda)$, in the visible spectral region from Pope & Fry (1997).

The absorption data from the HAW cruise characterize the potential scale of enhancement of particulate absorption coefficient and its phytoplankton and non-algal components under typical conditions of oligotrophic ocean, but including also an exceptional situation corresponding to the presence of a surface slick associated with a dense bloom of *Trichodesmium* (Fig. 7). The highest enhancement of $a_p(\lambda)$ in the SML was observed during the *Trichodesmium* bloom with the *EF* values as high as about 120 in the near-UV and the red (Fig. 7a). In the blue spectral region the *EF* dropped to values as low as 40. We note that at shorter UV wavelengths ($\lambda < 350$ nm, not shown in Fig. 7) we did not observe further increase in *EF*. For the remaining HAW samples the *EF* values for $a_p(\lambda)$ are also dependent on light wavelength and are still large although lower than for the *Trichodesmium* bloom. The lowest values of *EF* of 2.6 were observed in the blue spectral region for one of the samples from the open ocean station (9 Sep 2009). Another sample (30 Aug 2009) showed, however, significantly higher *EF*, ranging from about 14 in the 455–460 nm spectral band to 45 at 565–580 nm.

The spectral patterns of *EF* for phytoplankton absorption coefficient $a_{ph}(\lambda)$ (Fig. 7b) are similar to those for $a_p(\lambda)$. The highest values of *EF* for $a_{ph}(\lambda)$ exceed 200 in the near-UV and in the long-wavelength end of the visible spectrum for the *Trichodesmium* bloom. For other samples, the *EF* varies in the blue from 1.3 (13 Sep 2009) to 6 (30 Aug 2009) but can be as high as 24 at 560–570 nm (30 Aug 2009).

Except for the *Trichodesmium* bloom, the *EF* for the non-algal particulate absorption, $a_{NAP}(\lambda)$, exhibits a consistent spectral behavior of steady increase with light wavelength (Fig. 7c). In the short-wavelength end of the spectrum, the *EF* values for $a_{NAP}(\lambda)$ range from about 5 (9 Sep 2009) to 37 (30 Aug 2009). In the long-wavelength end of the spectrum the range is 8 to 70. In contrast to $a_p(\lambda)$ and $a_{ph}(\lambda)$, the *EF* values for $a_{NAP}(\lambda)$ for the *Trichodesmium* bloom are not higher than

those observed under typical open ocean conditions. These results reflect the dominant contribution of $a_{NAP}(\lambda)$ to $a_p(\lambda)$ in the SML and significantly higher enhancement of $a_{NAP}(\lambda)$ than $a_{ph}(\lambda)$ under oligotrophic ocean conditions off the Hawaiian Islands.

As the CDOM absorption data were not collected on the HAW cruise we cannot determine the enhancement of total absorption coefficient; however, Fig. 7d depicts the *EF* for the sum of $a_w(\lambda)$ and $a_p(\lambda)$. In this case, in addition to $a_w(\lambda)$ data from Pope & Fry (1997), we used $a_w(\lambda)$ in the short-wavelength and long-wavelengths ends of the spectrum from Sogandares & Fry (1997) and Smith & Baker (1981), respectively. Note that the spectral pattern for this *EF* is similar to that presented in Fig. 6d for the total absorption coefficient from the SBC cruise. For the HAW samples the sum $a_w(\lambda) + a_p(\lambda)$ is enhanced in the SML by as much as 50-fold in the near-UV for the *Trichodesmium* bloom and 10-fold at short visible wavelengths for one of the typical open ocean samples (30 Aug 2009). In the near-IR the *EF* values approach 1 (to within less than 1%).

3.3. Volume scattering function

Results from measurements of the particulate volume scattering function, $\beta_p(\psi)$, show that scattering by particles is significantly enhanced in the sea-surface microlayer compared with the underlying subsurface water (Fig. 8). This enhancement was observed within the entire range of scattering angles included in the measurements with LISST and DAWN instruments on the SBC samples (Fig. 8a,b) and DAWN on the HAW samples (Fig. 8c,d). We recall that the results obtained with DAWN can be viewed as conservative estimates of $\beta_p(\psi)$ because of potential underestimation of the contribution of relatively rare large particles. This is more likely to have some significance for the SML samples than USW samples because of greater enrichment of large particles in the SML (Fig. 3). We also note that the irregular variation seen in the three

most backward directions measured with DAWN (ψ = 134°, 141°, and 147°) is likely attributable to measurement uncertainties, including incomplete correction for reflection artifacts, rather than real features of $\beta_p(\psi)$ (Babin et al., 2012).

For comparison, Figure 8 displays the widely cited results obtained by Petzold (1972), which are representative of turbid water (data from San Diego Harbor) and clear ocean water (the Tongue of the Ocean, Bahama Islands). The Petzold data represent the spectral band centered at 514 nm (with a full width at half maximum of 75 nm) and illustrate a broad range of variability that encompasses our measurements of $\beta_p(\psi)$ for both the SML and USW samples. The lowest magnitude of $\beta_p(\psi)$ that we measured for the USW sample from waters off the Hawaiian Islands is somewhat higher than the Petzold clear water case (Fig. 8d). The highest magnitude of $\beta_p(\psi)$ that we measured for the SML samples on the HAW cruise (both during *Trichodesmium* bloom and in clear open ocean waters) is somewhat lower or comparable at backward scattering angles with the Petzold turbid water case (Fig. 8c,d). Our measurements also fall within a broad range of data collected more recently in 10 different coastal and oceanic environments by Sullivan & Twardowski (2009). For example, whereas in their dataset $\beta_p(90°)$ at 658 nm varies from about 7.5×10^{-5} to 1.5×10^{-2} m^{-1} sr^{-1}, the minimum and maximum values of $\beta_p(90°)$ at 532 nm in our measurements are 3.2×10^{-4} (the USW sample in Fig. 8d) and 6.1×10^{-3} m^{-1} sr^{-1} (the SML sample in Fig. 8c), respectively.

Figure 9 depicts $\beta_p(\psi)$ normalized to its value at ψ = 22.5° (i.e., the first forward detector of DAWN), which facilitates the illustration of differences in the angular shape of $\beta_p(\psi)$ between the SML and USW samples. As seen, for all measurements taken with DAWN on the SBC and HAW cruises a decrease of $\beta_p(\psi)$ with increasing scattering angle is less steep for the SML than USW samples. The forward scattering measurements of the SBC samples with the LISST

instrument also showed somewhat smaller steepness of $\beta_p(\psi)$ within the angular range 1° to 10° for the SML samples compared with the USW samples (not shown). Overall, the least steep function of $\beta_p(\psi)$, which implies the highest backscattering fraction, was measured on the SML sample collected under surface slick conditions during the *Trichodesmium* bloom (Fig. 9b). We note that the observed trends in the shape of $\beta_p(\psi)$ cannot be simply explained by our PSD data alone, which suggest that the SML samples have higher proportion of large particles than the USW samples, because this result would tend to increase rather than decrease the steepness of $\beta_p(\psi)$ in the SML. In addition to particle size, other particle characteristics such as shape, refractive index related to chemical composition, internal structure and heterogeneities, and the degree of particle aggregation are known to affect light scattering (Kerker et al., 1979; Meyer 1979; Morel & Bricaud, 1986; Mishchenko et al., 2000; Boss et al., 2009a). The effects associated with these factors may be reflected in our results although attention also needs to be called on unavoidable and difficult to quantify uncertainties of the techniques that we used for measuring particle size and light scattering (Slade & Boss, 2006; Jonasz & Fournier, 2007; Babin et al., 2012).

The enhancement of VSF in the SML is presented in Fig. 10. The results for the particulate component, $\beta_p(\psi)$, and the total VSF of seawater, $\beta(\psi)$, that includes both the molecular and particle contributions, are shown. As seen, the enhancement factor *EF* varies significantly between the samples and is also dependent on the scattering angle. The *EF* values are lower for the SBC samples (Fig. 10a) than HAW samples (Fig. 10b). In the Santa Barbara Channel the highest values of *EF* for β_p in the range 4 to 4.5 were measured for one sample (21 Sep 2008) at very small forward scattering angles (< 0.5°) and large angles (70°–130°). All SBC measurements show a conspicuous minimum of *EF* at forward scattering angles between 3° to 5°.

Note that beyond 5° there is a consistent increasing trend of *EF* showed by measurements with both LISST and DAWN. For the HAW samples the angular pattern of *EF* for β_p is characterized by a relatively broad maximum with a decreasing trend toward both ends of the DAWN angular range (Fig. 10b). Interestingly, in contrast to particulate absorption, the sample collected during the *Trichodesmium* bloom (27 Aug 2009) has the lowest magnitude of *EF* for particulate scattering among the three HAW samples. For this sample the maximum value of *EF* for β_p is 6.9 at $\psi = 81°$. The highest enhancement of β_p was observed in clear ocean waters off the Hawaiian Islands (30 Aug 2009) where *EF* exceeds 15 at scattering angles between about 65° and 80°.

For all examined samples the contribution of water molecular scattering, β_w, to total β at forward scattering angles was very small, for example < 2% at $\psi < 30°$ for the USW samples and < 2% at $\psi < 50°$ for the SML samples. As a result, at these forward angles the *EF* values for β_p and β are nearly the same (Fig. 10). At larger scattering angles the contribution of molecular scattering to β can become significant. For example, in the angular range 90° to 130° this contribution was 5% to 15% for the SML samples from the Santa Barbara Channel and 2 to 6% for the SML samples from the HAW cruise. Compared with the SML, the USW samples had consistently greater contribution of β_w to β. For most USW samples this contribution at scattering angles between 90° and 130° was 20% to 30%. The lowest and highest contributions were 11% (27 Aug 2009) and 34% (30 Aug 2009). Because of increased role of molecular scattering the *EF* values for β are smaller than those for β_p at large scattering angles (Fig. 10). Nevertheless, the enhancement of β remains large; for example, in the range 6 to 10 at $\psi = 90°$ for the HAW samples.

3.4. Degree of linear polarization

Figure 11 depicts results for the degree of linear polarization of light scattered by the SML and USW samples from the SBC and HAW cruises for both the particulate component of DoLP, $P_p(\psi)$, and the total DoLP of seawater, $P(\psi)$. For all samples the angular patterns of $P(\psi)$ and $P_p(\psi)$ have a characteristic bell shape with a maximum at side-scattering angles. Similar angular shape of DoLP was reported in previous measurements of seawater samples from different coastal and open ocean environments (Beardsley, 1968; Morel, 1973; Kadyshevich et al., 1976; Voss & Fry 1984), natural assemblages of marine particles (Koestner et al., 2018), different phytoplankton species (Fry & Voss, 1985; Quinby-Hunt et al., 1989; Volten et al., 1998; Zugger et al., 2008; Chami et al., 2014) as well as mineral particles, atmospheric dust and cosmic material (Weiss-Wrana, 1983; Volten et al., 2001; Chami et al. 2014).

In our experiments the maximum values of DoLP, denoted as P_{max} for the whole seawater samples and $P_{p,max}$ for particles, were measured with the side-scattering DAWN detectors centered at $\psi = 90°$ or 99°. The P_{max} values of the USW samples are highest among the cases presented in Fig. 11 although the differences are very small in the case of a dense surface bloom of *Trichodesmium* (Fig. 11d). The P_{max} values vary from 0.65 to 0.77 for the HAW samples and within a narrow range of 0.81 to 0.83 for the SBC samples. These observations are consistent with literature data and fall within a broader range of variability reported for a wide range of environments. For example, the average values of P_{max} of 0.7 (Kadyshevich et al., 1976) and 0.66 (Voss & Fry, 1984) were reported on the basis of measurements in the Atlantic and Pacific Oceans. Ivanoff et al. (1961) measured P_{max} within a range from about 0.38 in turbid shallow waters of Bermuda to 0.81 in clear waters of the Sargasso Sea.

The values of P_{max} are higher than $P_{p,max}$ because the pure seawater $P_{w,max}$ is generally higher

than the particulate $P_{p,max}$ and P_{max} is determined by the mixing rule (see Section 2.6.). However, because the contribution of β_w to β at side-scattering angles was small for the SBC samples, the P_{max} is higher than $P_{p,max}$ only by a few percent in this mesotrophic ocean environment (Fig. 11a,b,c). This difference is even smaller, less than 1%, for the *Trichodesmium* bloom (Fig.11d). In such cases when the β_w/β ratio is very small the changes in P_{max} are driven almost entirely by changes in $P_{p,max}$ with very little effect associated with relative contributions of water molecules and particles to light scattering. The largest differences between P_{max} and $P_{p,max}$ of about 14% and 8% are observed for two USW samples from clear oligotrophic waters where β_w/β at side-scattering angles was relatively high, 20% to 30% (Fig. 11e,f). In such cases the relative contributions of molecular and particulate scattering are expected to play a noticeable role in variations of P_{max} although changes in $P_{p,max}$ are still the dominant factor.

The most important finding presented in Fig 11 is that P_{max} and $P_{p,max}$ as well as the DoLP values in the angular vicinity of the maxima are significantly lower for the SML than the USW samples. This salient feature is observed for all examined samples (Fig. 11a,b,c,e,f) with the exception of the *Trichodesmium* bloom (Fig. 11d). For the SBC samples P_{max} of the SML ranges from 0.65 to 0.75 which corresponds to a 10% to 20% decrease compared with the USW (Fig. 11a,b,c). Similar percentages apply to a decrease in $P_{p,max}$. For the two HAW samples not representing the *Trichodesmium* bloom, the SML values of P_{max} dropped by 17% to a value of 0.53 (Fig. 11e) and 29% to 0.54 (Fig. 11f). The corresponding percentages for $P_{p,max}$ are somewhat smaller, 8% and 24% respectively. The particulate component of DoLP represents an inherent polarization property of particles so the observed significant decrease of $P_{p,max}$ in the SML compared with the USW is indicative of significant differences in the characteristics of particulate assemblages between the microlayer and the underlying bulk seawater. The particle

size, complex refractive index, shape, and internal structures have been implicated in interpretation of measured variability in particulate DoLP for various particle types (Weiss-Wrana, 1983; Volten et al., 1998, 2001; Chami et al., 2014). Our measurements of particle size distribution indicated an increased proportion of large-sized particles in the SML (Fig. 3) which can be associated with the observed decrease of the DoLP in the SML. Such trend between the DoLP and particle size has long been recognized (Hatch & Choate, 1930) and was also recently reported for natural particle assemblages from coastal and offshore waters of Southern California (Koestner et al., 2018). The potential effects associated with other particle characteristics cannot be assessed with available data but cannot be ruled out. For example, $P_{p,max}$ can decrease as a result of an increase in the refractive index of particles which, in turn, can be associated with an increased abundance of mineral particles (Volten et al., 1998, 2001; Chami et al., 2014). This possibility seems consistent with our findings that non-algal particles play a major role in particulate absorption in the SML, including significant absorption in the near-IR which, in turn, could be associated with an important role of atmospheric deposition of high-index particles.

As the SML samples show consistently higher magnitude of $\beta(\psi)$ and hence higher turbidity than the USW samples (Fig. 9), our results in Fig. 11 (except Fig. 11d) support earlier observations of a decreasing trend of P_{max} with increasing $\beta(90°)$, which was suggested to be associated with changes in particle properties, specifically from more polarizing in clear waters where large particles are relatively less abundant to less polarizing in turbid waters where large particles are more abundant (Ivanoff et al., 1961; Morel, 1973). This trend is not, however, observed under surface slick conditions during a dense bloom of *Trichodesmium* when the DoLP values for the SML and USW samples, including P_{max} and $P_{p,max}$, are all nearly the same (Fig. 11d). This is indicative of very similar polarization properties of particle assemblages in the

SML and USW samples despite large enhancements of particle scattering (Figs. 8c, 10b), absorption (Figs. 5a, 7), and concentration (Fig. 3) in the SML.

4. Summary and future perspectives

Whereas the sea-surface microlayer (SML) can be a site of significant enrichment for various classes of biogeochemically and optically significant materials, particulate species are expected to be typically the most consistently enriched because of stabilization of particles at the air-sea interface through surface tension forces. We observed consistent enrichment of particle concentration in the SML samples from the mesotrophic and oligotrophic oceanic environments. Whereas the highest observed value of the enrichment factor (*EF*) for the total concentration of particles larger than 0.7 μm was over 8 in clear open ocean oligotrophic waters off the Hawaiian Islands, the enrichment was also found to be a strong function of particle diameter with the highest values of size-dependent *EF* in the range of 30 to 70 for particle diameters between 10 μm and 30 μm observed in these oligotrophic waters. Under surface slick conditions during a dense bloom of *Trichodesmium* the *EF* values for large particles of 30 μm to 50 μm were even higher. In this case we also observed very high enrichment of 236-fold for Chla and 23-fold for POC.

The enhanced particle concentration and different size distribution in the SML compared with the underlying subsurface water (USW) are important factors that determine the inherent optical properties (IOPs) of the SML and the difference in these properties between the SML and USW. Our measurements in the mesotrophic waters of the Santa Barbara Channel showed higher enhancement factor for the spectral particulate absorption coefficient, $a_p(\lambda)$, than the CDOM absorption coefficient, $a_g(\lambda)$. The enhancement of absorption coefficients is generally dependent

on light wavelength and the highest *EF* for $a_p(\lambda)$ of about 120 was observed in the near-UV and the red portions of the spectrum during the surface bloom of *Trichodesmium* sampled near the Island of Hawaii. Under such conditions the phytoplankton absorption coefficient, $a_{ph}(\lambda)$, was enhanced over 200-fold in these spectral bands whereas the *EF* values for the non-algal particulate absorption coefficient, $a_{NAP}(\lambda)$, remained below 50 across the examined spectrum. In contrast, in typical open ocean oligotrophic waters we observed consistently higher enhancement for $a_{NAP}(\lambda)$ than $a_{ph}(\lambda)$. Under these conditions the *EF* values were as high as 24 for $a_{ph}(\lambda)$ in the green spectral region, 70 for $a_{NAP}(\lambda)$ in the long-wavelength end of the spectrum, 45 for $a_p(\lambda)$ in the green, and 10 for the total absorption coefficient of seawater, $a(\lambda)$, in the short-wavelength end of the visible spectrum. The enhancement of $a(\lambda)$ characteristically decreases with wavelength because of increasing role of pure water absorption.

In contrast to absorption, the particulate, $\beta_p(\psi)$, and total, $\beta(\psi)$, volume scattering functions (VSFs) measured within the range of intermediate and large scattering angles from about 20° to 150° were enhanced more in clear oligotrophic waters than in the situation of *Trichodesmium* bloom. The enhancement of VSFs was found to be a strong function of scattering angle ψ and the highest values of *EF* above 15 were observed for $\beta_p(\psi)$ at ψ between about 65° and 80°. For $\beta(\psi)$ the highest observed *EF* was about 13 for ψ between 50° and 65°. Interestingly, the angular shapes of particulate $\beta_p(\psi)$ suggest higher backscattering fraction in the SML than USW, which is inconsistent with the potential effect of observed higher enrichment of SML with large-sized particles than small-sized particles. Thus, it is likely that the differences in the shape of $\beta_p(\psi)$ between the SML and USW are associated largely with differences in the composition of particulate assemblages such as generally higher refractive index of particles in the SML than USW. This possibility appears to be consistent with higher enhancement of non-algal particulate

absorption compared with phytoplankton absorption which was observed under non-bloom oligotrophic conditions. It is conceivable that atmospheric deposition of minerogenic dust with relatively high refractive index plays an important role in the enhancement of non-algal particulate matter in the SML.

One of the most important results of this study is that for scattering angles in the vicinity of 90° we observed significantly lower values of the degree of linear polarization (DoLP) for light scattered by seawater, $P(\psi)$, as well as for light scattered by particles only, $P_p(\psi)$, in the SML compared with USW. This result was observed consistently in both the mesotrophic and oligotrophic environments with the exception of extreme conditions of surface bloom of *Trichodesmium* for which the DoLP values were nearly the same in the SML and USW. Our data from clear oligotrophic waters off the Hawaiian Islands indicate that the contrast between the SML and USW in terms of maximum DoLP occurring typically at ψ between 90° and 100° can be as high as 30%. Although this contrast decreases toward forward and backward scattering angles, this finding may have implications for the modification of the state of polarization of both the downwelling light as it enters the ocean through the SML and the water-leaving upwelling light as it enters the atmosphere through the SML. Thus, the inherent polarization properties of the sea surface microlayer may have to be considered in the development of approaches based on the use of remote-sensing optical polarimetry from satellite and airborne platforms for the study of seawater constituents present in the bulk surface waters. This point is important in view of increasing interest in such approaches over recent years, especially in the context of future satellite missions (Chami, 2007; Loisel et al., 2008; Harmel, 2016; Ibrahim et al., 2016; Werdell et al., 2018).

Whereas the thinness of the SML does not prevent its potentially significant effect on the

state of polarization of light crossing the air-water interface, one can expect very little attenuation of light propagating through a very short path length of microlayer. To provide quantitative insight into this question we estimated the spectral attenuation coefficient for downward plane irradiance, $K_d(\lambda)$, for the microlayer assuming the IOPs measured during a dense surface bloom of *Trichodesmium* (sample from 27 Aug 2009). We note that this case was characterized by the highest magnitude of absorption coefficient and volume scattering function among all microlayer samples examined in this study. In this estimation we used the approximate formula that links $K_d(\lambda)$ with IOPs: $K_d(\lambda) = 1.0395\ [a(\lambda) + b_b(\lambda)]/\mu_d(\lambda)$, where $a(\lambda)$ and $b_b(\lambda)$ are the absorption and backscattering coefficients of seawater and $\mu_d(\lambda)$ is the average cosine of downwelling light just below the sea surface (Gordon 1989). In these calculations we assumed $\mu_d(\lambda) = 0.85$ which is reasonable for clear sky conditions and low solar zenith angle (Li et al. 2019). For the $a(\lambda)$ values we assumed the sum of $a_w(\lambda)$ and our measured values of $a_p(\lambda)$. We ignored the contribution of CDOM because these measurements were not made at the station of interest. Finally, for the $b_b(\lambda)$ values we used the sum of pure seawater, $b_{bw}(\lambda)$, and particulate, $b_{bp}(\lambda)$, contributions. The latter was estimated from our DAWN measurements of $\beta_p(\psi)$ at 532 nm, which were first extrapolated to $\psi = 180°$ using the method of Beardsley & Zaneveld (1969) and then integrated to yield b_{bp} at 532 nm. The spectral values of $b_{bp}(\lambda)$ were then obtained assuming that this coefficient varies as λ^{-1}.

The results of these calculations are depicted in Fig. 12 and indicate large enhancement (> 10-fold) in the SML of $K_d(\lambda)$ in the near-UV and blue spectral regions (Fig. 12a) and a very small attenuation loss of downward irradiance as the light crosses the SML (Fig. 12b). In the calculation of this loss a 1-mm thickness of the SML was assumed. As seen, for such short path length the percent transmittance of downward irradiance differs from 100% only by a fraction of

1% within the examined spectral range.

Whereas the above calculations provide one simple example of potential usefulness of information on IOPs of the SML, such information can be useful in a broader context of more advanced radiative transfer studies aimed, for instance, at quantitative assessment of potential effects of the SML on ocean reflectance and related remote-sensing applications. In addition, the IOPs have long been demonstrated to provide useful information about concentration-related and composition-related characteristics of various constituents of bulk seawater such as dissolved organic matter (e.g., Bricaud et al., 1981; Vodacek et al., 1997; Mannino et al., 2008), Chla, POC, SPM (e.g., Carder et al., 1974; Bricaud et al., 1998; Loisel & Morel, 1998; Stramski et al., 2008; Boss et al., 2009b), and particle size and composition (e.g., Boss et al., 2001; Twardowski et al., 2001; Loisel et al., 2007; Woźniak et al., 2010; Slade & Boss, 2015). Similarly, the measurements of optical absorption and scattering properties including polarization properties of the SML have the unique potential to extend the observational capabilities for characterizing the constituents of the SML. Recent reviews of sea-surface microlayer research points to a need of multidisciplinary research initiatives to improve an understanding of physical, chemical and biological processes in the SML and effectively address several crucial questions associated with their consequences for the Earth system (Cunliffe et al., 2013; Engel et al., 2017). The measurements of the optical properties of the SML, which were largely ignored in the past but have been shown in this study to be highly variable in contrasting oceanic environments, can provide a significant added value for such multidisciplinary research initiatives.

Acknowledgements

This study was supported by the Radiance in a Dynamic Ocean (RaDyO) program of the US Office of Naval Research (ONR grant N00014-06-1-0071 awarded to Dariusz Stramski). Financial support was also provided through a postdoctoral scholarship (WU 585/2-1) awarded to Oliver Wurl by the Deutsche Forschungsgemeinschaft. We also thank Svein Vagle for supporting the participation of Oliver Wurl in this study (ONR grant N00014-07-1-0754). The CHN analysis of samples was done by the Marine Science Institute at UC Santa Barbara, California. The HPLC pigment analysis of samples collected on the Hawaiian cruise was done by Laboratoire d'Océanographie in Villefranche-sur-Mer, France. We thank scientists who participated in the RaDyO field campaigns and the officers and crew of *R/V Kilo Moana* for their invaluable support and logistical assistance. We also thank Xiaodong Zhang and four anonymous reviewers for providing helpful comments on the manuscript.

References

Adams, J. T., E. Aas, N. Højerslev, and B. Lundgren. 2002. Comparison of radiance and polarization values in the Mediterranean Sea and simulated in the Monte Carlo model. Appl. Opt. **41**: 2724–2733.

Agogué, H., E. O. Casamayor, F. Joux, I. Obernosterer, C. Dupuy, F. Lantoine, P. Catala, M. G. Weinbauer, T. Reinthaler, G. J. Herndl, and P. Lebaron. 2004. Comparison of samplers for the biological characterization of the sea surface microlayer. Limnol. Oceanogr. Methods **2**: 213–225.

Agrawal, Y. C. 2005. The optical volume scattering function: Temporal and vertical variability in the water column off the New Jersey coast. Limnol. Oceanogr. **50***:*1787–1794.

Agrawal, Y. C. and O. A. Mikkelsen. 2009. Empirical forward scattering phase functions from 0.08 to 16 deg for randomly shaped terrigenous 1–21 μm sediment grains. Opt. Express **17**: 8805–8814.

Agrawal, Y. C. and H. C. Pottsmith. 2000. Instruments for particle size and settling velocity observations in sediment transport. Mar. Geol. **168**: 89–114.

Andrews, S. W., D. M. Nover, K. E. Reardon, J. E. Reuter, and S. G. Schladow. 2011. The influence of ambient light intensity on in situ laser diffractometers. Water Resour. Res. **47**: W06509, doi:10.1029/2010WR009841.

Arimoto, R., W. L. Balsam, and C. Schloesslin. 2002. Visible spectroscopy of aerosol particles collected on filters: iron-oxide minerals. Atmos. Environ. **36**: 89–96.

Babin, M. and D. Stramski. 2002. Light absorption by aquatic particles in the near-infrared spectral region. Limnol. Oceanogr. **47**: 911–915.

Babin, M. and D. Stramski. 2004. Variations in the mass-specific absorption coefficient of mineral particles suspended in water. Limnol. Oceanogr. **49**: 756–767.

Babin, M., D. Stramski, R. A. Reynolds, V. M. Wright, and E. Leymarie. 2012. Determination of the volume scattering function of aqueous particle suspensions with a laboratory multi-angle light scattering instrument. Appl. Opt. **51**: 3853–3873.

Bader, H. 1970. The hyperbolic distribution of particle sizes. J. Geophys. Res. **75**: 2822–2830.

Beardsley, G. F., Jr. 1968. Mueller scattering matrix of sea water. J. Opt. Soc Am. **58**: 52–57.

Beardsley, G.F. Jr., and J. R. V. Zaneveld. 1969. Theoretical dependence of the near-asymptotic apparent optical properties on the inherent optical properties of sea water. J. Opt. Soc. Am. **58**: 373–377.

Bickel, W. S. and W. M. Bailey. 1985. Stokes vectors, Mueller matrices, and polarized scattered light. Am. J. Phys. **53**: 468–478.

Bohren, C. F. and D. R. Huffman. 1983. Absorption and Scattering of Light by Small Particles. John Wiley&Sons.

Bond, T. C. and R. W. Bergstrom. 2006. Light absorption by carbonaceous particles: An investigative review. Aerosol Sci. Tech. **40**: 27–67.

Boss, E., W. H. Slade, and P. Hill. 2009a. Effect of particulate aggregation in aquatic environments on the beam-attenuation and its utility as a proxy for particulate mass. Opt. Express **17**: 9408–9420.

Boss, E.; L. Taylor, S. Gilbert, K. Gundersen, N. Hawley, C. Janzen, T. Johengen, H. Purcell, C. Robertson, D. W. Schar, G. J. Smith, and M. N. Tamburri. 2009b. Comparison of inherent optical properties as a surrogate for particulate matter concentration in coastal waters. Limnol. Ocean. Methods **7**: 803–810.

Boss, E., M. S. Twardowski, and S. Herring. 2001. Shape of the particulate beam attenuation spectrum and its relation to the size distribution of oceanic particles. Appl. Opt. **40**: 4885–4893.

Bricaud, A., A. Morel, M. Babin, K. Allali, and H. Claustre. 1998. Variations of light absorption by suspended particles with chlorophyll *a* concentration in oceanic (case 1) waters: Analysis and implications for bio-optical models. J. Geophys. Res. **103**: 31033–31044.

Bricaud, A., A. Morel, and L. Prieur. 1981. Absorption by dissolved organic matter of the sea (yellow substance) in the UV and visible domains. Limnol. Oceanogr. **26**: 43–53.

Bricaud, A. and D. Stramski. 1990. Spectral absorption coefficients of living phytoplankton and nonalgal biogenous matter: a comparison between the Peru upwelling area and the Sargasso

Sea. Limnol. Oceanogr. **35**: 562–582.

Carder, K. L., P. R. Betzer, and D. W Eggimann. 1974. Physical, chemical and optical measures of suspended-particle concentrations: Their intercomparison and application to the West African Shelf. In: Gibbs, J. (ed.), Suspended Solids in Water, Plenum, pp. 173–193.

Carlson, D. J. 1982. A field evaluation of plate and screen microlayer sampling techniques. Mar. Chem. **11**: 189–208.

Carlson, D. J. 1983. Dissolved organic materials in surface microlayers*:* Temporal and spatial variability and relation to sea state. Limnol. Oceanogr. **28**: 415–431.

Chami, M. 2007. Importance of the polarization in the retrieval of oceanic constituents from the remote sensing reflectance. J. Geophys. Res. **112**: C05026. doi:10.1029/2006JC003843.

Chami, M., A. Thirouard, and T. Harmel. 2014. POLVSM (Polarized Volume Scattering Meter) instrument: an innovative device to measure the directional and polarized scattering properties of hydrosols. Opt. Express **22**(21): 26403–26428. doi:10.1364/OE.22.026403

Cunliffe, M., A. Engel, S. Frka, B. Gašparovic, C. Guitart, J. C. Murrell, M. Salter, C. Stolle, R. Upstill-Goddard, and O. Wurl. 2013. Sea surface microlayers: a unified physicochemical and biological perspective of the air–ocean interface. Prog. Oceanogr. **109**: 104–116.

Cunliffe, M. and J. C. Murrell. 2009. The sea surface microlayer is a gelatinous biofilm. The ISME Journal **3**: 1001–1003, doi:10.1038/ismej.2009.69.

Cunliffe, M., R. C. Upstill-Goddard, and J. C. Murrell. 2011. Microbiology of aquatic surface microlayers. FEMS Microbiol. Rev. **35**: 233–246.

Daumas, R. A., P. L. Laborde, J. C. Marty, and A. Saliot. 1976. Influence of sampling method on the chemical composition of water surface film. Limnol. Oceanogr. **21**: 319–326.

Dickey, T., M. Banner, P. Bhandari, T. Boyd, L. Carvalho, G. Chang, Y. Chao, H. Czerski, M.

Darecki, C. Dong, D. Farmer, S. Freeman, J. Gemmrich, P. Gernez, N. Hall-Patch, B. Holt, S. Jiang, C. Jones, G. Kattawar, D. LeBell, L. Lenain, M. Lewis, Y. Liu, L. Logan, D. Manov, W. K. Melville, M. A. Moline, R. Morison, F. Nencioli, W. S. Pegau, B. Reineman, I. Robbins, R. Röttgers, H. Schultz, L. Shen, M. Shinki, M. Slivkoff, M. Sokólski, F. Spada, N. Statom, D. Stramski, P. Sutherland, M. Twardowski, S. Vagle, R. Van Dommelen, K. Voss, L. Washburn, J. Wei, H. Wijesekera, O. Wurl, , D. Yang, S. Yildiz, Y. You, D. K. P. Yue, R. Zaneveld, and C. J. Zappa. 2012. Introduction to special section on Recent Advances in the Study of Optical Variability in the Near-Surface and Upper Ocean. J. Geophys. Res. **117**: C00H20, doi:10.1029/2012JC007964.

Engel, A., H. W. Bange, M. Cunliffe, S. M. Burrows, G. Friedrichs, L. Galgani, H. Herrmann, N. Hertkorn, M. Johnson, P. S. Liss, P. K. Quinn, M. Schartau, A. Soloviev, C. Stolle, R. C. Upstill-Goddard, M. van Pinxteren, and B. Zäncker. 2017. The ocean's vital skin: Toward an integrated understanding of the sea surface microlayer. Front. Mar. Sci. **4**: 165. doi:10.3389/fmars.2017.00165.

Estep, K. W., J. S. Maki, S. C. Danos, and C. C. Remsen. 1985. The retrieval of material from the surface microlayer with screen and plate samplers and its implications for partitioning of material within the microlayer. Freshwater Biol. **15**: 15–19.

Ferrari, G.M. and S. Tassan. 1999. A method using chemical oxidation to remove light absorption by phytoplankton pigments. J. Phycol. **35:** 1090–1098.

Fry, E. S. and K. J. Voss. 1985. Measurement of the Mueller matrix for phytoplankton. Limnol. Oceanogr. **30**: 1322–3326.

Galgani, L. and A. Engel. 2016. Changes in optical characteristics of surface microlayers hint to photochemically and microbially mediated DOM turnover in the upwelling region off the

coast of Peru. Biogeosciences **13**: 2453–2473.

Gilerson, A. A., J. Stepinski, A. I. Ibrahim, Y. You, J. M. Sullivan, M. S. Twardowski, H. M. Dierssen, B. Russell, M. E. Cummings, P. Brady, S. A. Ahmed, and G. W. Kattawar. 2013. Benthic effects on the polarization of light in shallow waters. Appl. Opt. **52**: 8685–8705.

Gordon, H. R. 1989. Can the Lambert-Beer law be applied to the diffuse attenuation coefficient of ocean water? Limnol. Oceanogr. **34**: 1389-1409.

Hardy, J. T. 1982. The sea-surface microlayer - biology, chemistry and anthropogenic enrichment. Prog. Oceanogr. **11**: 307–328.

Hardy, J. T. and C. W. Apts. 1989. Photosynthetic carbon reduction: High rates in the sea-surface microlayer. Mar. Biol. 101: 411–417.

Harmel, T., 2016. Recent developments in the use of light polarization for marine environment monitoring from space. In: Kokhanovsky, A. A. (ed.), Light Scattering Reviews 10, Springer, pp. 41–84.

Harvey, G. W. and L. A. Burzell. 1972. A simple microlayer method for small samples. Limnol. Oceanogr. **17**: 156–157.

Hatch, T. and S. P. Choate. 1930. Measurement of polarization of the Tyndall beam of aqueous suspension as an aid in determining particle size. J. Franklin Inst**. 210**: 793–804.

Hovenier, J. W.; H. Volten, O. Muñoz, W. J. Van der Zande, and L. B. F. M. Waters. 2002. Laboratory studies of scattering matrices for randomly oriented particles. Potentials, problems, and perspectives. J. Quant. Spectrosc. Radiat. Transf. **79–80**: 741–755.

Hunter, K. A. 1980. Processes affecting particulate trace metals in the sea surface microlayer. Mar. Chem. **9**: 49–70.

Hunter, K. A. 2005 Chemistry of the sea-surface microlayer. In: Liss, P. S. and Duce, R. A.

(eds.), Sea Surface and Global Change. Cambridge University Press, pp. 287–319.

Ibrahim, A., A. Gilerson, J. Chowdhary, and S. Ahmed. 2016. Retrieval of macro- and micro-physical properties of oceanic hydrosols from polarimetric observations. Remote Sens. Environ. **186**: 548–566.

Ivanoff, A. 1974. Polarization measurements in the sea. In: Jerlov, N. G. and Steeman-Nielsen, E. (eds.), Optical Aspects of Oceanography, Academic Press, pp. 151–175.

Ivanoff, A., N. Jerlov, and T. H. Waterman. 1961. A comparative study of irradiance, beam transmittance and scattering in the sea near Bermuda. Limnol. Oceanogr. **6**: 129–148.

Jonasz, M. and G. Fournier. 2007. Light Scattering by Particles in Water. Theoretical and Experimental Foundations, Elsevier.

Joux, F., H. Agogué, I. Obernosterer, C. Dupuy, T. Reinthaler, G. J. Herndl, and P. Lebaron. 2006. Microbial community structure in the sea surface microlayer at two contrasting sites in the Northwestern Mediterranean Sea. Aquat. Microb. Ecol. **42**: 91–104.

Kadyshevich, Y. A., Y. S. Lyubovtseva, and G. V. Rozenberg. 1976. Light-scattering matrices of Pacific and Atlantic ocean waters. Izv. Acad. Sci. USSR Atmos. Oceanic Phys. **12**: 106–111.

Kerker, M., H. Chew, P. J. McNulty, J. P. Kratohvil, D. D. Cooke, M. Sculley, and M.-P Lee. 1979. Light scattering and fluorescence by small particles having internal structure. J. Histochem. Cytochem. **27**: 250–263.

Kishino, M., M. Takahashi, N. Okami, and S. Ichimura. 1985. Estimation of spectral absorption coefficients of phytoplankton in the sea. Bull. Mar. Sci. **37**: 634–42.

Koestner, D., D. Stramski, and R. A. Reynolds. 2018. Measurements of the volume scattering function and the degree of linear polarization of light scattered by contrasting natural assemblages of marine particles. Appl. Sci. **8**(12): 2690. doi:10.3390/app8122690.

Kokhanovsky, A. A. 2003. Parameterization of the Mueller matrix of oceanic waters. J. Geophys. Res. **108**(C6): 3175, doi:10.1029/2001JC001222.

Knap, A., A. Michaels, A. Close, H. Ducklow, and A. Dickson. 1996. Protocols for the Joint Global Ocean Flux Study (JGOFS) Core Measurements, JGOFS Report Nr. 19 (Reprint of the IOC Manuals and Guides No. 29, UNESCO, Paris, 1994), 170 pp.

Lefering, I., R. Röttgers, C. Utschig, and D. McKee. 2017. Uncertainty budgets for liquid waveguide CDOM absorption measurements. Appl. Opt. **56**: 6357–6366.

Li, L., D. Stramski, and M. Darecki. 2018. Characterization of the light field and apparent optical properties in the ocean euphotic layer based on hyperspectral measurements of the irradiance quartet. Appl. Sci. **8**(12): 2677. doi:10.3390/app8122677.

Lindberg, J. D. 1975. The composition and optical absorption coefficient of atmospheric particulate matter. Opt. Quantum Electron. **7**: 131–139.

Lindberg, J. D., R. E. Douglass, and D. M. Garvey. 199. Carbon and the optical properties of atmospheric dust, Appl. Opt. **32**: 6077–6081.

Liss, P. S. 1975. Chemistry of the sea-surface microlayer. In: Riley, J. P. and Skirrow, G. S. (eds.), Chemical Oceanography, 2nd ed., Vol. 2, Academic Press, pp. 193–243.

Liss, P. S. and R. A. Duce. 2005. The Sea Surface and Global Change. Cambridge University Press.

Loisel, H., L. Duforêt, D. Dessailly, M. Chami, and P. Dubuisson. 2008. Investigation of the variations in the water leaving polarized reflectance from the POLDER satellite data over two biogeochemical contrasted oceanic areas. Opt. Express **16**: 12905–12918.

Loisel, H., X. Mériaux, J. F. Berthon, and A. Poteau. 2007. Investigation of the optical backscattering to scattering ratio of marine particles in relation with their biogeochemical

composition in the eastern English Channel and southern North Sea. Limnol. Oceanogr. **52**: 739–752.

Loisel, H. and A. Morel. 1998. Light scattering and chlorophyll concentration in case 1 waters: A reexamination. Limnol. Oceanogr. **43**: 847–858.

MacIntyre, F. 1974. The top millimeter of the ocean. Sci. Am. **230**(5): 62–77.

Mannino, A., M. E. Russ, and S. B. Hooker. 2008. Algorithm development and validation for satellite-derived distributions of DOC and CDOM in the U.S. Middle Atlantic Bight. J. Geophys. Res. **113**, C07051, doi:10.1029/2007JC004493.

Meyer, R. A. 1979. Light scattering from biological cells: Dependence of backscatter radiation on membrane thickness and refractive index. Appl. Opt. **18**: 585–588.

Mishchenko, M. I., J. W. Hovenier, and L. D. Travis. 2000. Light Scattering by Nonspherical Particles. Theory, Measurements, and Applications. Academic Press.

Mitchell, B. G. 1990. Algorithm for determining the absorption coefficient of aquatic particulates using the quantitative filter technique (QFT). in: R.W. Spinrad, R. W. (ed.), Ocean Optics X, Proc. SPIE **1302**, The Society of Photo-Optical Instrumentation Engineers, Bellingham, WA, pp. 137–148.

Mobley, C. D. 1994. Light and Water: Radiative Transfer in Natural Waters. Academic Press.

Morel, A. 1973. Diffusion de la lumière par les eaux de mer, Résultats expérimentaux et approche théorique. In: Optics of the Sea (Interface and In-Water Transmission and Imaging), AGARD Lecture Series No. 61, North Atlantic Treaty Organization, pp. 3.1-1–3.1-76.

Morel, A. and Y-H. Ahn. 1991. Optics of heterotrophic nanoflagellates and ciliates: A tentative assessment of their scattering role in oceanic waters compared to those of bacterial and algal cells. J. Mar. Res. **49**: 1–12.

Morel, A. and A. Bricaud. 1986. Inherent optical properties of algal cells including picoplankton: theoretical and experimental results. in: T. Platt and Li, W. K. W. (eds.), Photosynthetic Picoplankton, Can. Bull. Fish. Aquat. Sci. **214**: 521–559.

Obernosterer, I., P. Catala, R. Lami, J. Caparros, J. Ras, A. Bricaud, C. Dupuy, F. van Wambeke, and P. Lebaron. 2008. Biochemical characteristics and bacterial community structure of the sea surface microlayer in the S. Pacific Ocean. Biogeosciences 5: 693–705, doi:10.5194/bg-5-693-2008.

Parsons, T. R., Y. Maita, and C. M Lalli. 1984. A Manual of Chemical and Biological Methods for Seawater Analysis, Elsevier.

Petrova, E. V., K. Jockers, N. N. Kiselev. 2000. Light scattering by aggregates with sizes comparable to the wavelength: An application to cometary dust. Icarus **148**: 526–536.

Pope, R. M. and E. S. Fry. 1997. Absorption spectrum (380-700 nm) of pure water. II. Integrating cavity measurements. Appl. Opt. **36**: 8710–8723.

Quinby-Hunt, M. S., A. J. Hunt, K. Lofftus, and D. Shapiro. 1989. Polarized-light scattering studies of marine Chlorella. Limnol. Oceanogr. **34**: 1587–1600.

Ras, J., J. Uitz, and H. Claustre. 2008. Spatial variability of phytoplankton pigment distributions in the Subtropical South Pacific Ocean: comparison between in situ and modelled data. Biogeosciences **5**: 353-369.

Ritchie, R. J. 2008. Universal chlorophyll equations for estimating chlorophylls a, b, c, and d and total chlorophylls in natural assemblages of photosynthetic organisms using acetone,

methanol, or ethanol solvents. Photosynthetica **46**: 115–126.

Reynolds, R. A., D. Stramski, V. M. Wright, and S. B. Woźniak. 2010. Measurements and characterization of particle size distributions in coastal waters. J. Geophys. Res. **115**: C08024, doi:10.1029/2009JC005930.

Roesler, C., D. Stramski, E. J. D'Sa, R. Röttgers, and R. A. Reynolds. 2018. Spectrophotometric measurements of particulate absorption using filter pads. In: Neeley, A. R. and Mannino, A. (eds.), IOCCG Ocean Optics and Biogeochemistry Protocols for Satellite Ocean Colour Sensor Validation, Volume 1, Inherent Optical Property Measurements and Protocols: Absorption Coefficient, International Ocean-Colour Coordinating Group, pp. 50–73.

Röttgers, R. 2018. Point-source integrating cavity absorption meters. In: Neeley, A. R. and Mannino, A. (eds.), IOCCG Ocean Optics and Biogeochemistry Protocols for Satellite Ocean Colour Sensor Validation, Volume 1, Inherent Optical Property Measurements and Protocols: Absorption Coefficient, International Ocean-Colour Coordinating Group, pp. 43–49.

Röttgers, R. and R. Doerffer. 2007. Measurements of optical absorption by chromophoric dissolved organic matter using a point-source integrating-cavity absorption meter. Limnol. Oceanogr. Methods **5**: 126–135.

Röttgers, R. and S. Gehnke. 2012. Measurement of light absorption by aquatic particles: improvement of the quantitative filter technique by use of an integrating sphere approach. Appl. Opt. **51**: 1336–1351.

Röttgers, R., C. Häse, and R. Doerffer. 2007. Determination of the particulate absorption of microalgae using a point-source integrating-cavity absorption meter: verification with a photometric technique, improvements for pigment bleaching and correction for chlorophyll fluorescence. Limnol. Oceanogr. Methods **5**: 1–12.

Schuster, G. L., O. Dubovik, B. N. Holben, and E. E. Clothiaux. 2005. Inferring black carbon content and specific absorption from Aerosol Robotic Network (AERONET) aerosol retrievals, J. Geophys. Res. **110**: D10S17, doi: 10.1029/2004JD004548.

Shinki, M., M. Wendeberg, S. Vagle, J. T. Cullen, and D. K. Hore. 2012. Characterization of adsorbed microlayer thickness on an oceanic glass plate sampler. Limnol. Oceanogr. Methods: **10**: 728–735.

Sieburth, J. McN. 1983. Microbiological and organic–chemical processes in the surface and mixed layers. In: Liss, P. S. and Slinn, W. G. N. (eds.), Air–Sea Exchange of Gases and Particles. Reidel Publishers, pp. 121–172.

Slade, W. H. and E. S. Boss. 2006. Calibrated near-forward volume scattering function obtained from the LISST particle sizer**.** Opt. Express **14(8)**: 3602–3615.

Slade, W. H. and E. Boss. 2015. Spectral attenuation and backscattering as indicators of average particle size. Appl. Opt. **54**: 7264-7277.

Sogandares, F. M. and E. S. Fry. 1997. Absorption spectrum (340-640 nm) of pure water. I. Photothermal measurements. Appl. Opt. **36**: 8699–8709.

Smith, R. C. and K. S. Baker. 1981. Optical properties of the clearest natural waters (200-800 nm. Appl. Opt. **20**: 177–184.

Soloviev, A. and R. Lukas. 2014. The Near-Surface Layer of the Ocean, Structure, Dynamics and Applications, 2nd ed., Atmospheric and Oceanographic Sciences Library 48, Springer.

Stramska, M., D. Stramski, M. Cichocka, A. Cieplak, and S. B. Woźniak. 2008. Effects of atmospheric particles from Southern California on the optical properties of seawater. J. Geophys. Res. **113**: C08037, doi:10.1029/2007JC004407.

Stramski, D., M. Babin, and S. B. Woźniak. 2007. Variations in the optical properties of terrigeneous mineral-rich particulate matter suspended in seawater. Limnol. Oceanogr. **52**: 2418–2433.

Stramski, D. and D. A. Kiefer. 1991. Light scattering by microorganisms in the open ocean. Prog. Oceanogr. **28**: 343–383.

Stramski, D., R. A. Reynolds, M. Babin, S. Kaczmarek, M. R. Lewis, R. Röttgers, A. Sciandra, M. Stramska, M. S. Twardowski, B. A. Franz, and H. Claustre. 2008. Relationships between the surface concentration of particulate organic carbon and optical properties in the eastern South Pacific and eastern Atlantic Oceans. Biogeosciences **5**: 171–201.

Stramski, D., R. A. Reynolds, S. Kaczmarek, J. Uitz, and G. Zheng. 2015. Correction of pathlength amplification in the filter-pad technique for measurements of particulate absorption coefficient in the visible spectral region. Appl. Opt. **54**: 6763–6782.

Stramski, D., S. B. Woźniak, and P. J. Flatau. 2004. Optical properties of Asian mineral dust suspended in seawater. Limnol. Oceanogr. **49**: 749–755.

Sullivan, J. M. and M. S. Twardowski. 2009. Angular shape of the oceanic particulate volume scattering function in the backward direction. Appl. Opt. **48**: 6811–6819.

Tilstone, G. H., R. L. Airs, V. Martinez-Vicente, C. Widdicombe, and C. Llewellyn. 2010. High concentrations of mycosporine-like amino acids and colored dissolved organic matter in the sea surface microlayer off the Iberian Peninsula. Limnol. Oceanogr. **55**: 1835–1850.

Twardowski M., E. Boss, J. B. MacDonald, W. S. Pegau, A. H. Barnard, and J. R. V. Zaneveld. 2001. A model for estimating bulk refractive index from the optical backscattering ratio and the implications for understanding particle composition in case I and case II waters. J. Geophys. Res. **106**: 129–142.

Van der Linde, D. W. 1998. Protocol for determination of total suspended matter in oceans and coastal zones. Technical Note No. 1.98.182, CEC-JRC, 8 pp.

Van Heukelem, L., and C. S. Thomas. 2001. Computer-assisted high-performance liquid chromatography method development with applications to the isolation and analysis of phytoplankton pigments. J. Chromatogr. A **910**: 31–49.

Vodacek, A., N. V. Blough, M. D. DeGrandpre, E. T. Peltzer, and R. K. Nelson. 1997. Seasonal variation of CDOM and DOC in the Middle Atlantic Bight: Terrestrial inputs and photooxidation, Limnol. Oceanogr. **42**: 674–686.

Volten, H., J. F. De Haan, J. W. Hovenier, R. Schreurs, W. Vassen, A. G. Dekker, H. J. Hoogenboom, F. Charlton, and R. Wouts. 1998. Laboratory measurements of angular distributions of light scattered by phytoplankton and silt. Limnol. Oceanogr. **43**: 1180–1197.

Volten, H., O. Muñoz, E. Rol, J. D. Haan, W. Vassen, J. W. Hovenier, and T. Nousiainen. 2001. Scattering matrices of mineral aerosol particles at 441.6 nm and 632.8 nm. J. Geophys. Res. **106**: 17375–17401.

Voss, K. J. and E. S. Fry. 1984. Measurement of the Mueller matrix for ocean water. Appl. Opt. **23**: 4427–4439.

Wangersky, P. J. 1976. The surface film as a physical environment. Ann. Rev. Ecol. Syst. **7**: 161–176.

Waterman, T. H. 1954. Polarization patterns in submarine illumination. Science **120**: 927–932.

Weiss-Wrana, K. 1983. Optical properties of interplanetary dust: comparison with light scattering by larger meteoritic and terrestrial grains. Astron. Astrophys. **126**: 240–250.

Werdell, J. P., L. I. W. McKinna, E. Boss, S. G. Ackleson, S. E. Craig., W. W. Gregg, Z. Lee, S. Maritorena, C. S. Roesler, C. S. Rousseaux, D. Stramski, J. M. Sullivan, M. S. Twardowski,

M. Tzortziou, and X. Zhang. 2018. An overview of approaches and challenges for retrieving marine inherent optical properties from ocean color remote sensing. Prog. Oceanogr. **160**: 186–212.

Woźniak, S. B., D. Stramski, M. Stramska, R. A. Reynolds, V. M. Wright, E. Y. Miksic, M. Cichocka, and A. M. Cieplak. 2010. Optical variability of seawater in relation to particle concentration, composition, and size distribution in the nearshore marine environment at Imperial Beach, California. J. Geophys. Res. **115**: C08027, doi:10.1029/2009JC005554.

Wurl, O., W. Ekau, W. M. Landing, and C. J. Zappa. 2017. Sea surface microlayer in a changing ocean - A perspective. Elem. Sci. Anth. **5**: 31, doi:10.1525/elementa.228.

Wurl, O. and M. Holmes. 2008. The gelatinous nature of the sea-surface microlayer. Mar. Chem. **110**: 89–97.

Wurl, O., L. Miller, R. Röttgers, and S. Vagle. 2009. The distribution and fate of surface-active substances in the sea-surface microlayer and water column. Mar. Chem. **115**: 1–9.

Wurl, O., L. Miller, and S. Vagle. 2011a. Production and fate of transparent exopolymer particles in the ocean. J. Geophys. Res. **116**: C00H13, doi:10.1029/2011JC007342.

Wurl, O., E. Wurl, L. Miller, K. Johnson, and S. Vagle. 2011b. Formation and global distribution of sea surface microlayers. Biogeosciences **8**: 121–135.

Zaitsev, Y. P. 1971. Marine Neustonology (translated from Russian). National Marine Fisheries Service, NOAA and NSF, 270 pp.

Zäncker, B., A. Bracher, R. Röttgers, and A. Engel. 2017. Variations of organic matter composition in the sea surface microlayer: A comparison between open ocean, coastal, and upwelling sites off the Peruvian coast. Front. Microbiol. **8**: 2369. doi:10.3389/fmicb.2017.02369.

Zhang, X., L. Hu, and M.-X. He. 2009. Scattering by pure seawater: Effect of salinity. Opt. Express **17**: 5698–5710.

Zhang, X., D. Stramski, R. A. Reynolds, and E. R. Blocker. 2019. Light scattering by pure water and seawater: the depolarization ratio and its variation with salinity. Appl. Opt. **58**: 991–1004.

Zugger, M. E., A. Messmer, T. J. Kane, J. Prentice, B. Concannon, A. Laux, and L. Mullen. 2008. Optical scattering properties of phytoplankton: Measurements and comparison of various species at scattering angles between 1° and 170°. Limnol. Oceanogr. **53**: 381–386.

Figure captions

Figure 1. Example particle size distributions measured on samples of the sea-surface microlayer (SML) and underlying subsurface water (USW) in the Santa Barbara Channel. **(a)** and **(c)** Density function of particle number concentration, F_N. **(b)** and **(d)** Density function of particle volume distribution, F_V. Data collected on 20 Sep 2008 [**(a)** and **(b)**] and 21 Sep 2008 [**(c)** and **(d)**] are shown. The power law function $F_N \sim D^{-4}$ is shown for comparison with measured particle number distributions.

Figure 2. As Figure 1 but for measurements taken off the Hawaiian Islands. **(a)** and **(b)** Data collected on 27 Aug 2009 near the Island of Hawaii during a dense surface bloom of *Trichodesmium*. **(c)** and **(d)** Data collected on 30 Aug 2009 in open ocean oligotrophic waters.

Figure 3. Enrichment factor (*EF*) for particle concentration of the sea-surface microlayer as a function of particle diameter. **(a)** Data collected in the Santa Barbara Channel on 20 Sep 2008 (solid black line), 21 Sep 2008 (dotted black line), and 22 Sep 2008 (solid gray line). **(b)** Data collected off the Hawaiian Islands on 27 Aug 2009 (solid black line), 28 Aug 2009 (dotted black line), and 30 Aug 2009 (solid gray line).

Figure 4. Example spectra of the absorption coefficients measured on samples of the sea-surface microlayer (SML) and underlying subsurface water (USW) in the Santa Barbara Channel. **(a)** The absorption coefficient of colored dissolved organic matter, $a_g(\lambda)$. **(b)** The absorption coefficient of suspended particulate matter, $a_p(\lambda)$. Both measurements were taken on 21 Sep 2008. The difference spectra between the SML and USW measurements are also shown.

Figure 5. Example spectra of the absorption coefficients measured on samples of the sea-surface microlayer (SML) and underlying subsurface water (USW) off the Hawaiian Islands. **(a)** and **(d)** The absorption coefficient of suspended particulate matter, $a_p(\lambda)$. **(b)** and **(e)** The absorption coefficient of non-algal particulate matter, $a_{NAP}(\lambda)$. **(c)** and **(f)** The absorption coefficient of phytoplankton, $a_{ph}(\lambda)$. **(a)**, **(b)**, **(c)** Data collected on 27 Aug 2009 near the Island of Hawaii during a dense surface bloom of *Trichodesmium*. The insets show data in the UV spectral range. **(d)**, **(e)**, **(f)** Data collected on 30 Aug 2009 in open ocean oligotrophic waters. In all panels data for the USW samples are multiplied by 10 to facilitate graphical comparison. The data of $a_{NAP}(\lambda)$ and $a_{ph}(\lambda)$ were obtained with the methanol extraction method but the dashed lines in **(b)** and **(c)** show additional results of absorption partitioning obtained with a bleaching method.

Figure 6. Enhancement factor (*EF*) for the spectral absorption coefficients of the sea-surface microlayer in the Santa Barbara Channel. **(a)** *EF* for the absorption coefficient of colored dissolved organic matter, $a_g(\lambda)$. **(b)** *EF* for the absorption coefficient of suspended particulate matter, $a_p(\lambda)$. **(c)** *EF* for the sum of $a_g(\lambda)$ and $a_p(\lambda)$. **(d)** *EF* for the total absorption coefficient of seawater, $a(\lambda)$. Different line types represent data collected on different days as indicated.

Figure 7. Enhancement factor (*EF*) for the spectral absorption coefficients of the sea-surface microlayer off the Hawaiian Islands. **(a)** *EF* for the absorption coefficient of suspended particulate matter, $a_p(\lambda)$. **(b)** *EF* for the absorption coefficient of phytoplankton, $a_{ph}(\lambda)$. Unlike other panels no data is shown past 700 nm because values of $a_{ph}(\lambda)$ in the near-infrared are very close to zero **(c)** *EF* for the absorption coefficient of non-algal particulate matter, $a_{NAP}(\lambda)$. **(d)** *EF*

for the sum of $a_p(\lambda)$ and pure water absorption, $a_w(\lambda)$. Different line types represent data collected on different days as indicated.

Figure 8. Example data of particulate volume scattering function, β_p, obtained from measurements on samples of the sea-surface microlayer (SML) and underlying subsurface water (USW). **(a)** and **(b)** Data collected in the Santa Barbara Channel on 20 Sep 2008 and 21 Sep 2008, respectively. **(c)** and **(d)** Data collected off the Hawaiian Islands on 27 Aug 2009 during a dense surface bloom of *Trichodesmium* and 30 Aug 2009 in open ocean oligotrophic waters, respectively. The insets are included in **(a)** and **(b)** to facilitate illustration in the range of scattering angles > 20^o. For comparison, in all panels data of Petzold (1972) are also shown as indicated.

Figure 9. Comparison of normalized particulate volume scattering functions, $\beta_p(\psi)/\beta_p(22.5°)$, for the sea surface microlayer (SML) and underlying subsurface water (USW). **(a)** Data collected in the Santa Barbara Channel on 20 Sep 2008, 21 Sep 2008, and 22 Sep 2008. **(b)** Data collected off the Hawaiian Islands on 27 Aug 2009, 28 Aug 2009, and 30 Aug 2009.

Figure 10. Enhancement factor (*EF*) for particulate volume scattering function β_p (black curves), and total volume scattering function of seawater β (gray curves) in the sea-surface microlayer as a function of scattering angle. **(a)** Data collected in the Santa Barbara Channel on 20 Sep 2008 (solid black line), 21 Sep 2008 (dotted black line), and 22 Sep 2008 (solid gray line). **(b)** Data collected off the Hawaiian Islands on 27 Aug 2009 (solid black line), 28 Aug 2009 (dotted black line), and 30 Aug 2009 (solid gray line).

Figure 11. The degree of linear polarization of light scattered by suspended particles, P_p, and whole seawater samples, P, as a function of scattering angle for the sea-surface microlayer (SML) and underlying subsurface water (USW). **(a)**, **(b)**, **(c)** Data collected in the Santa Barbara Channel on the days as indicated. **(d)**, **(e)**, **(f)** Data collected off the Hawaiian Islands on the days as indicated.

Figure 12. (a) Estimates of the enhancement factor (*EF*) for the diffuse attenuation coefficient of downward irradiance, K_d, in the sea-surface microlayer as a function of light wavelength. **(b)** Estimates of the spectral transmittance of downward irradiance, T_d, through a 1-mm thick microlayer based on the estimates of spectral K_d within the microlayer. All presented estimates are based on measurements of the inherent optical properties of the SML and USW samples collected during a surface bloom of *Trichodesmium* near the Island of Hawaii (27 Aug 2009).

Table 1. Summary of data illustrating the range of concentrations of chlorophyll-*a* (Chla), particulate organic carbon (POC), suspended particulate matter (SPM), total particle number integrated over the size range measured with the Coulter technique (N_{total}), as well as the ratio POC/SPM for samples of underlying subsurface water (USW) collected in the Santa Barbara Channel and off the Hawaiian Islands. Data for the enrichment factor (*EF*) in the sea-surface microlayer (SML) are also shown for the cases when measurements for both SML and USW were done. n/d indicates "not determined".

	Santa Barbara Channel		**off Hawaiian Islands**	
		EF		*EF*
Chla [mg m^{-3}]	0.99 – 1.03	n/d	0.057 – 0.089	236*
POC [mg m^{-3}]	164 – 289	1.6 – 2.6	34 – 96	23*
SPM [mg m^{-3}]	484 – 555	n/d	92 – 140	n/d
N_{total} [m^{-3}]	1.3 – 1.6 x 10^{11}	1.3 – 2.2	6.5 – 8.1 x 10^{10}	3.0 – 8.7
POC/SPM [g / g]	0.36 – 0.52	n/d	0.36 – 0.51	n/d

* data based on measurements during a dense surface bloom of *Trichodesmium*

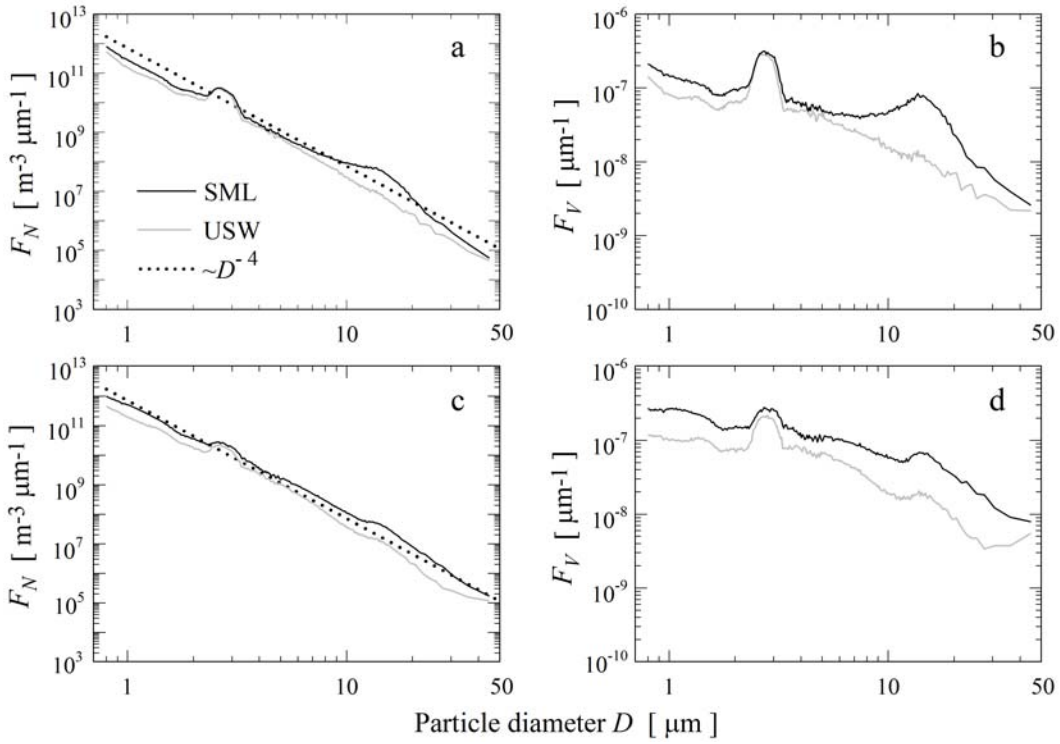

1420

Figure 1. Example particle size distributions measured on samples of the sea-surface microlayer (SML) and underlying subsurface water (USW) in the Santa Barbara Channel. **(a)** and **(c)** Density function of particle number concentration, F_N. **(b)** and **(d)** Density function of particle

1425 volume distribution, F_V. Data collected on 20 Sep 2008 [**(a)** and **(b)**] and 21 Sep 2008 [**(c)** and **(d)**] are shown. The power law function $F_N \sim D^{-4}$ is shown for comparison with measured particle number distributions.

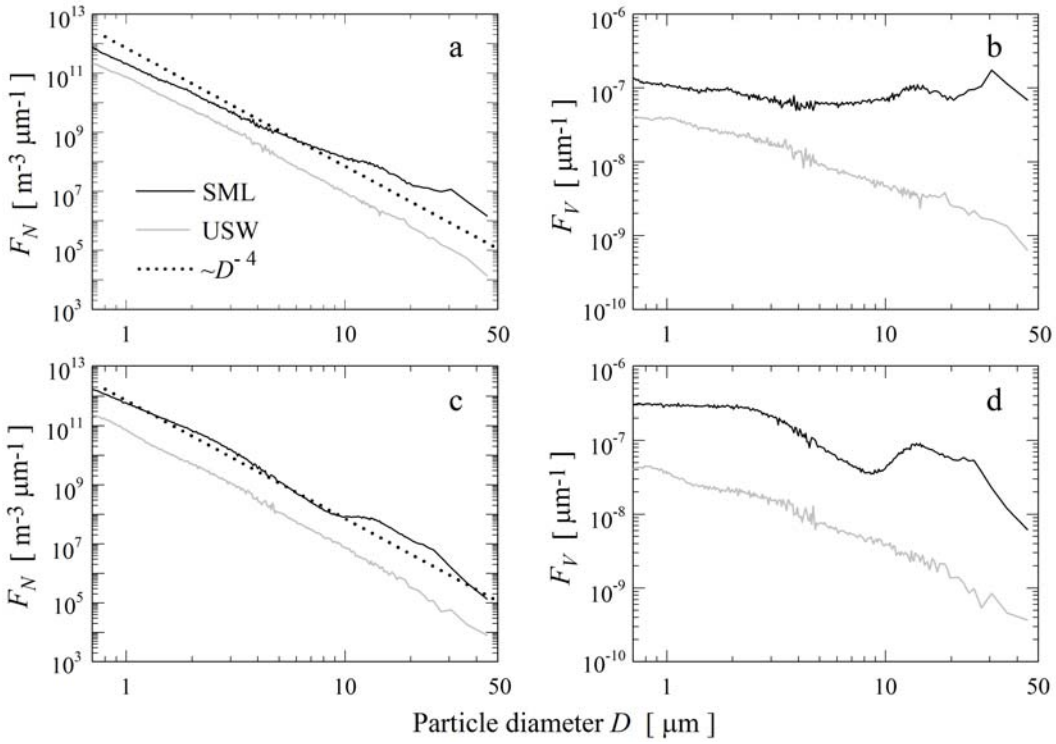

1430

Figure 2. As Figure 1 but for measurements taken off the Hawaiian Islands. **(a)** and **(b)** Data collected on 27 Aug 2009 near the Island of Hawaii during a dense surface bloom of *Trichodesmium*. **(c)** and **(d)** Data collected on 30 Aug 2009 in open ocean oligotrophic waters.

1435

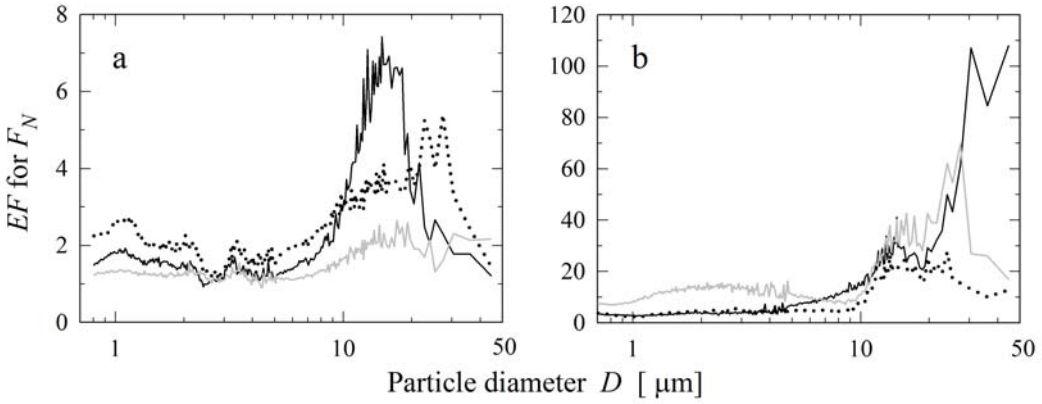

Figure 3. Enrichment factor (*EF*) for particle concentration of the sea-surface microlayer as a function of particle diameter. **(a)** Data collected in the Santa Barbara Channel on 20 Sep 2008 (solid black line), 21 Sep 2008 (dotted black line), and 22 Sep 2008 (solid gray line). **(b)** Data collected off the Hawaiian Islands on 27 Aug 2009 (solid black line), 28 Aug 2009 (dotted black line), and 30 Aug 2009 (solid gray line).

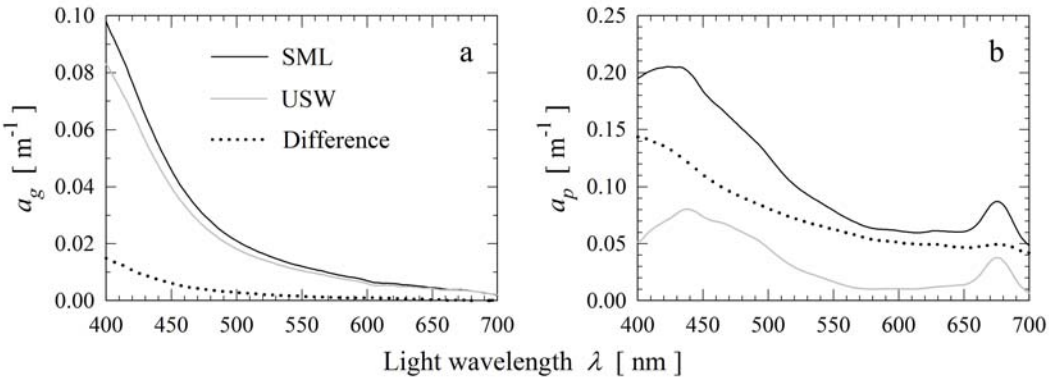

Figure 4. Example spectra of the absorption coefficients measured on samples of the sea-surface microlayer (SML) and underlying subsurface water (USW) in the Santa Barbara Channel. **(a)** The absorption coefficient of colored dissolved organic matter, $a_g(\lambda)$. **(b)** The absorption coefficient of suspended particulate matter, $a_p(\lambda)$. Both measurements were taken on 21 Sep 2008. The difference spectra between the SML and USW measurements are also shown.

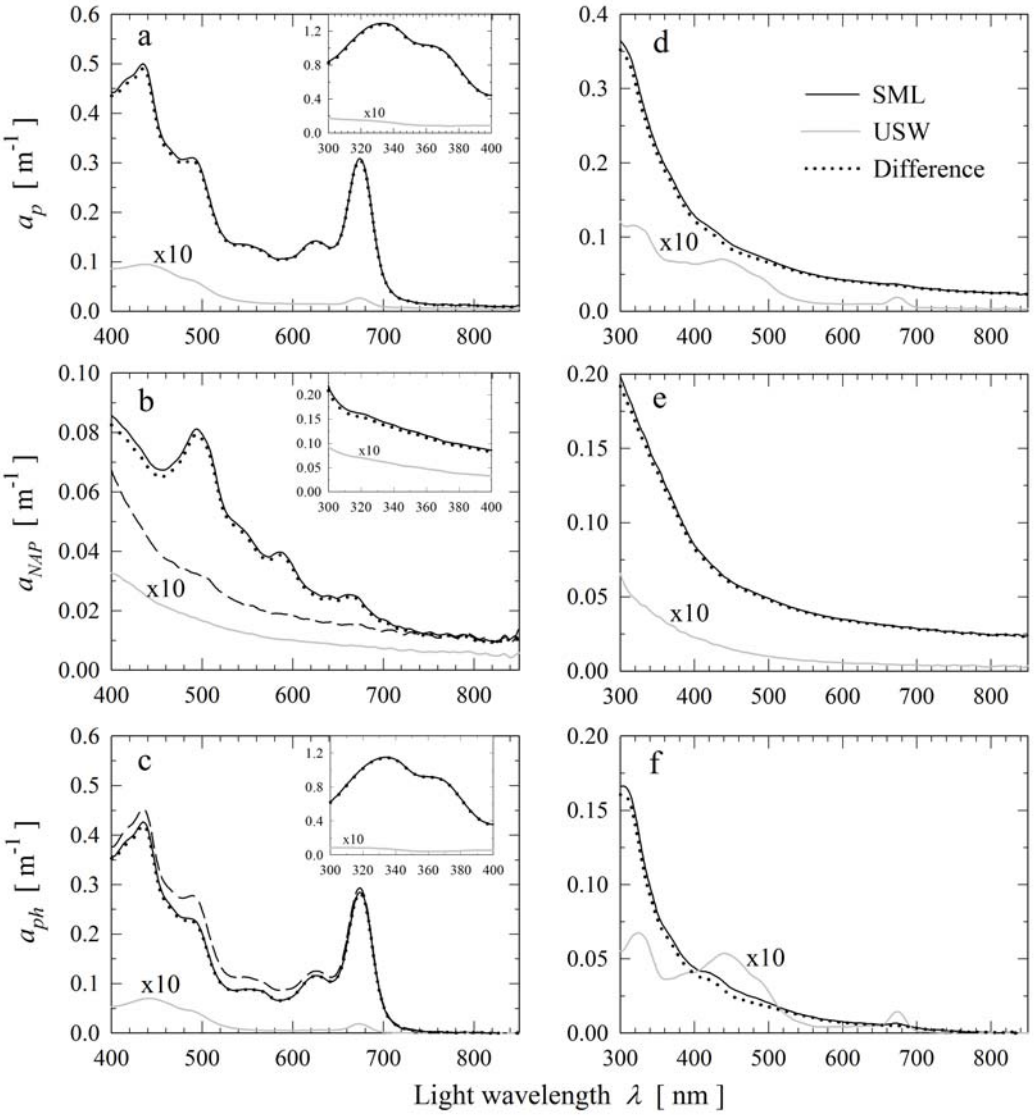

1455

Figure 5. Example spectra of the absorption coefficients measured on samples of the sea-surface microlayer (SML) and underlying subsurface water (USW) off the Hawaiian Islands. **(a)** and **(d)** The absorption coefficient of suspended particulate matter, $a_p(\lambda)$. **(b)** and **(e)** The absorption

1460 coefficient of non-algal particulate matter, $a_{NAP}(\lambda)$. **(c)** and **(f)** The absorption coefficient of phytoplankton, $a_{ph}(\lambda)$. **(a)**, **(b)**, **(c)** Data collected on 27 Aug 2009 near the Island of Hawaii during a dense surface bloom of *Trichodesmium*. The insets show data in the UV spectral range. **(d)**, **(e)**, **(f)** Data collected on 30 Aug 2009 in open ocean oligotrophic waters. In all panels data

for the USW samples are multiplied by 10 to facilitate graphical comparison. The data of $a_{NAP}(\lambda)$ and $a_{ph}(\lambda)$ were obtained with the methanol extraction method but the dashed lines in **(b)** and **(c)** show additional results of absorption partitioning obtained with a bleaching method.

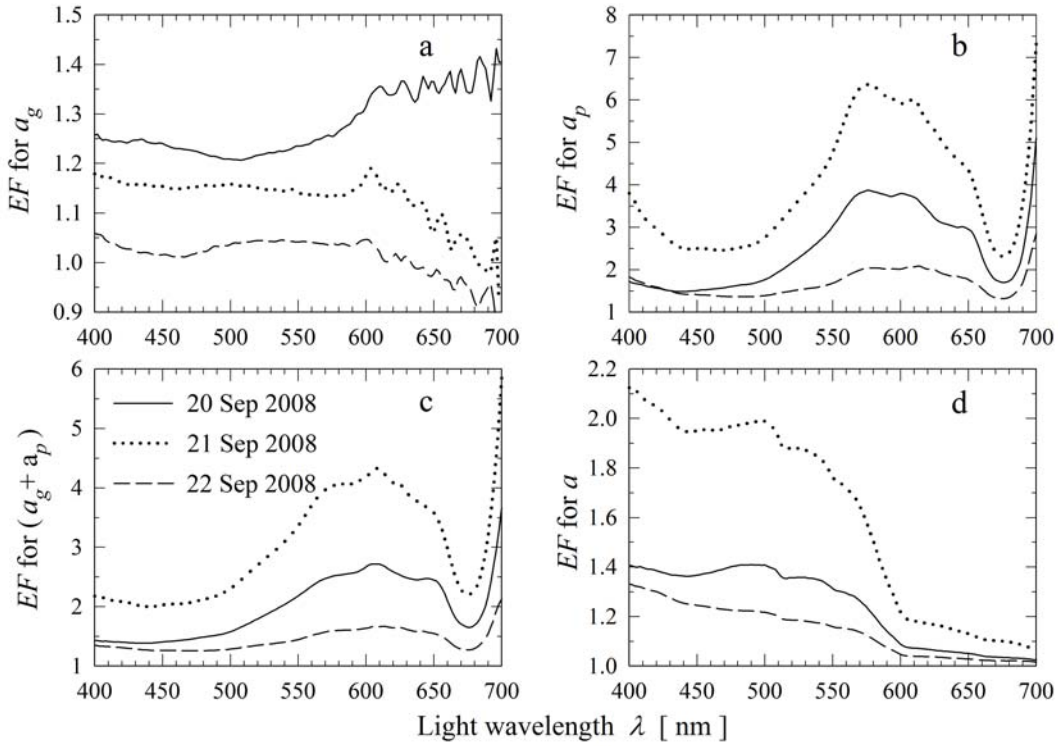

Figure 6. Enhancement factor (*EF*) for the spectral absorption coefficients of the sea-surface microlayer in the Santa Barbara Channel. **(a)** *EF* for the absorption coefficient of colored dissolved organic matter, $a_g(\lambda)$. **(b)** *EF* for the absorption coefficient of suspended particulate matter, $a_p(\lambda)$. **(c)** *EF* for the sum of $a_g(\lambda)$ and $a_p(\lambda)$. **(d)** *EF* for the total absorption coefficient of seawater, $a(\lambda)$. Different line types represent data collected on different days as indicated.

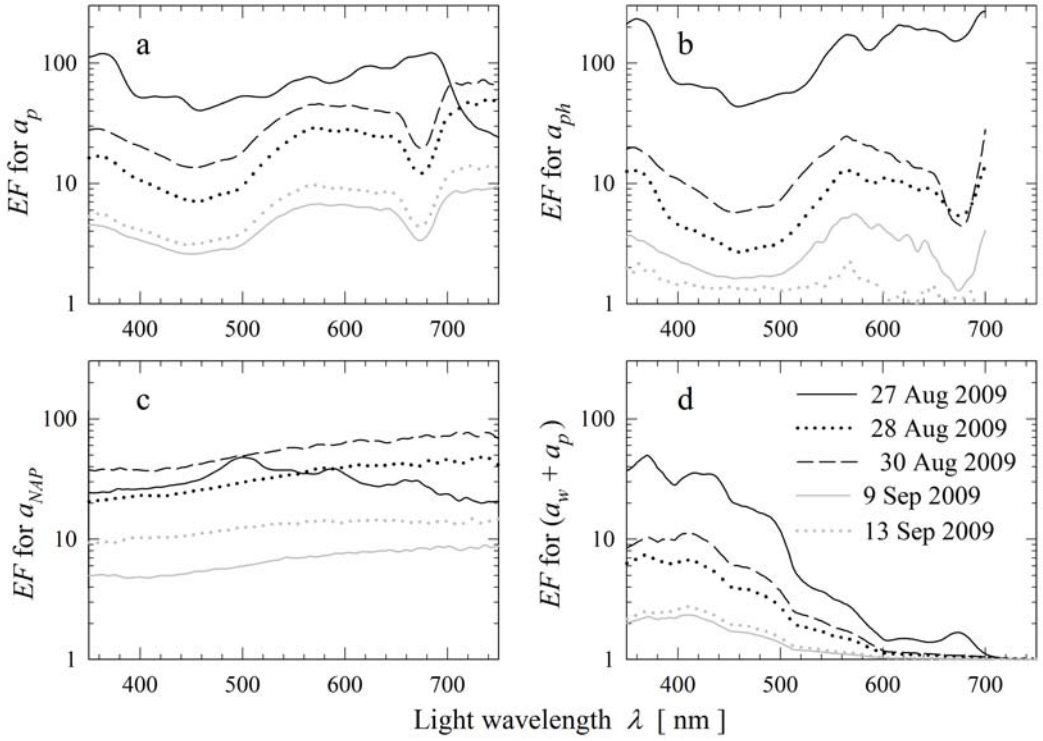

Figure 7. Enhancement factor (*EF*) for the spectral absorption coefficients of the sea-surface microlayer off the Hawaiian Islands. **(a)** *EF* for the absorption coefficient of suspended particulate matter, $a_p(\lambda)$. **(b)** *EF* for the absorption coefficient of phytoplankton, $a_{ph}(\lambda)$. Unlike other panels no data is shown past 700 nm because values of $a_{ph}(\lambda)$ in the near-infrared are very close to zero **(c)** *EF* for the absorption coefficient of non-algal particulate matter, $a_{NAP}(\lambda)$. **(d)** *EF* for the sum of $a_p(\lambda)$ and pure water absorption, $a_w(\lambda)$. Different line types represent data collected on different days as indicated.

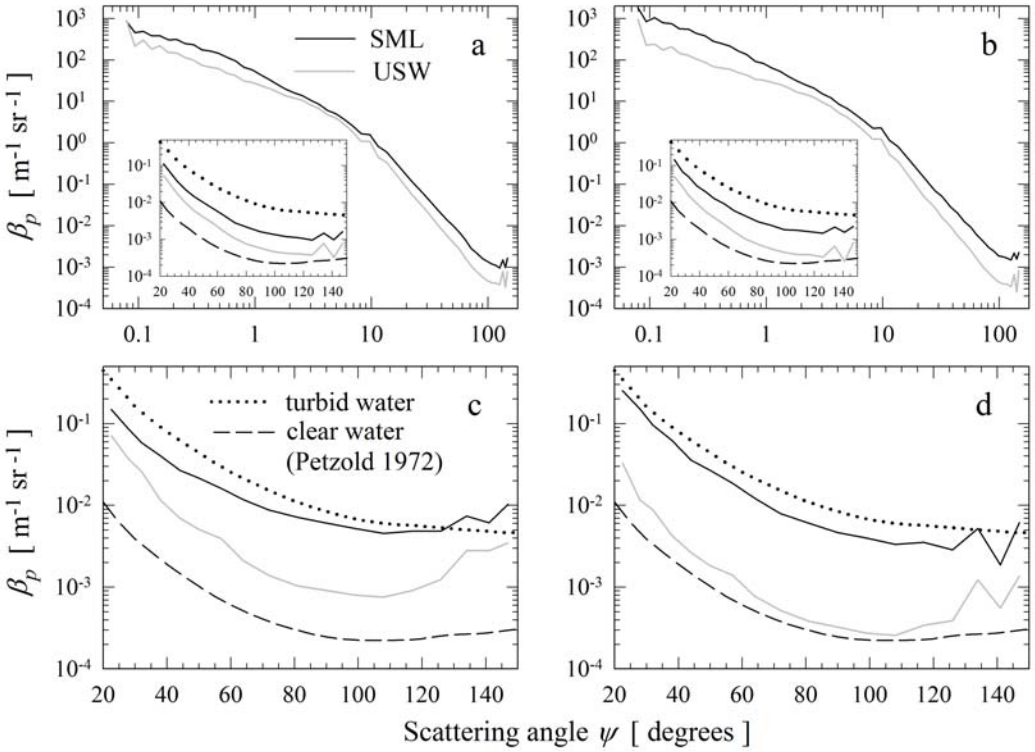

1490

Figure 8. Example data of particulate volume scattering function, β_p, obtained from measurements on samples of the sea-surface microlayer (SML) and underlying subsurface water (USW). **(a)** and **(b)** Data collected in the Santa Barbara Channel on 20 Sep 2008 and 21 Sep 2008, respectively. **(c)** and **(d)** Data collected off the Hawaiian Islands on 27 Aug 2009 during a

1495 dense surface bloom of *Trichodesmium* and 30 Aug 2009 in open ocean oligotrophic waters, respectively. The insets are included in **(a)** and **(b)** to facilitate illustration in the range of scattering angles > 20^o. For comparison, in all panels data of Petzold (1972) are also shown as indicated.

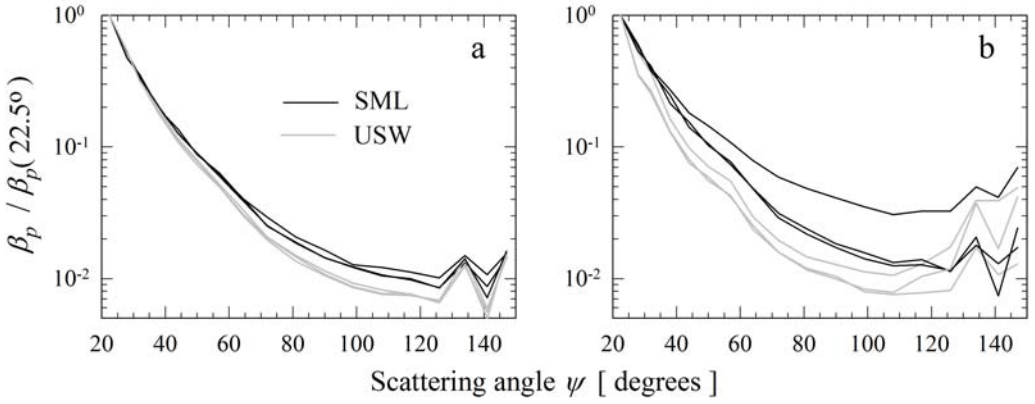

Figure 9. Comparison of normalized particulate volume scattering functions, $\beta_p(\psi)/\beta_p(22.5°)$, for the sea surface microlayer (SML) and underlying subsurface water (USW). **(a)** Data collected in the Santa Barbara Channel on 20 Sep 2008, 21 Sep 2008, and 22 Sep 2008. **(b)** Data collected off the Hawaiian Islands on 27 Aug 2009, 28 Aug 2009, and 30 Aug 2009.

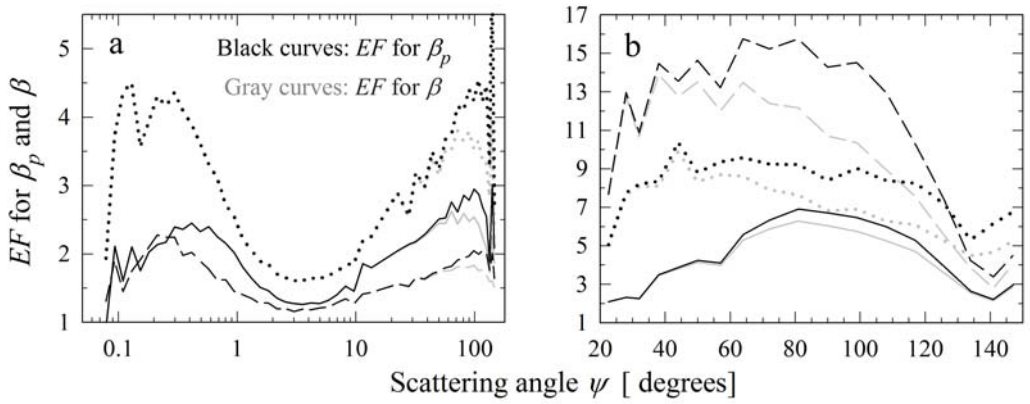

1510

Figure 10. Enhancement factor (*EF*) for particulate volume scattering function β_p (black curves), and total volume scattering function of seawater β (gray curves) in the sea-surface microlayer as a function of scattering angle. **(a)** Data collected in the Santa Barbara Channel on 20 Sep 2008 (solid black line), 21 Sep 2008 (dotted black line), and 22 Sep 2008 (solid gray line). **(b)** Data

1515 collected off the Hawaiian Islands on 27 Aug 2009 (solid black line), 28 Aug 2009 (dotted black line), and 30 Aug 2009 (solid gray line).

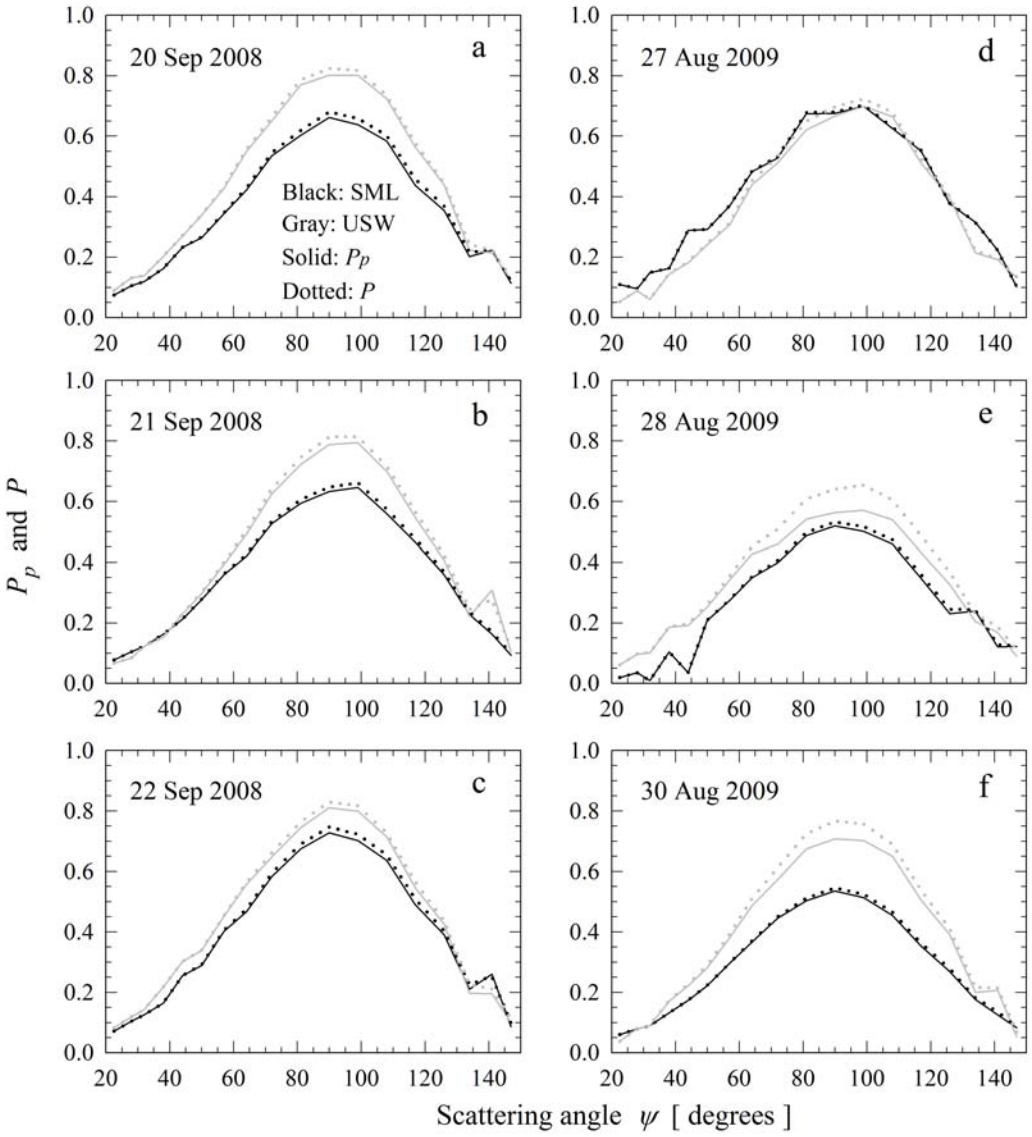

Figure 11. The degree of linear polarization of light scattered by suspended particles, P_p, and whole seawater samples, P, as a function of scattering angle for the sea-surface microlayer (SML) and underlying subsurface water (USW). **(a)**, **(b)**, **(c)** Data collected in the Santa Barbara Channel on the days as indicated. **(d)**, **(e)**, **(f)** Data collected off the Hawaiian Islands on the days as indicated.

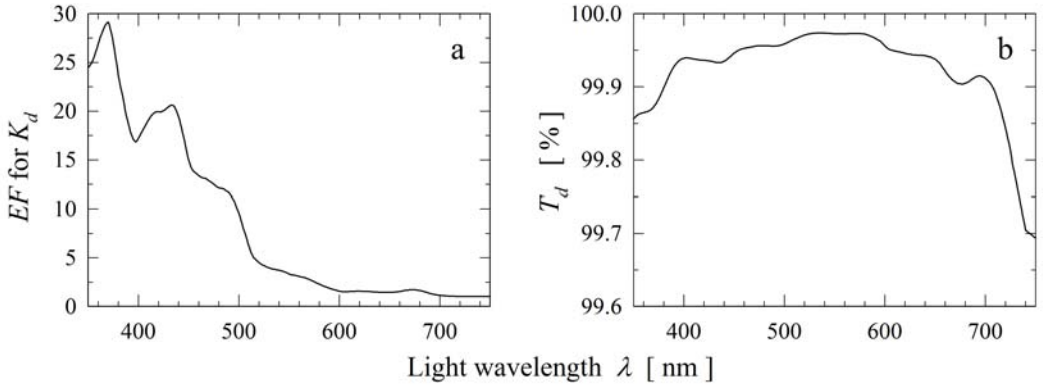

Figure 12. (a) Estimates of the enhancement factor (*EF*) for the diffuse attenuation coefficient of downward irradiance, K_d, in the sea-surface microlayer as a function of light wavelength. **(b)** Estimates of the spectral transmittance of downward irradiance, T_d, through a 1-mm thick microlayer based on the estimates of spectral K_d within the microlayer. All presented estimates are based on measurements of the inherent optical properties of the SML and USW samples collected during a surface bloom of *Trichodesmium* near the Island of Hawaii (27 Aug 2009).